Magazine of Concrete Research, 2002, **54**, No. 2, April, 77–101

Modelling of heated concrete

G. A. Khoury,* C. E. Majorana,† F. Pesavento† and B. A. Schrefler†

Imperial College; University of Padua

This paper presents the basic principles and details of the physical, mathematical and numerical models forming the main structure of the numerical analysis of the thermal, hydral and mechanical behaviour of normal, high-performance and ultra-high performance concrete structures subjected to heating. A fully coupled non-linear formulation is designed to predict the behaviour and potential for spalling, of heated concrete structures for fire and nuclear reactor applications. Concrete is considered as a multiphase material consisting of a solid phase, two gas phases and three water phases. The physical model is described with emphasis being placed upon the real processes occurring in concrete during heated based on tests carried out in several major laboratories around Europe as part of the wider HITECO research programme. Examples of preliminary outputs are presented in the form of isoline diagrams compared with those obtained from experiment.

Notation

b	adsorbed physically bound water
$\boldsymbol{b}$	body force vector
C_p	effective specific heat of concrete (J kg^{-1} K^{-1})
C_{pga}	specific heat of dry air (J kg^{-1} K^{-1})
C_{pgwa}	specific heat of moist air (J kg^{-1} K^{-1})
C_{pw}	specific heat of free water (J kg^{-1} K^{-1})
D	damage parameter
E_a	activation energy
g	gas phase
m	moisture
p_c	capillary pressure (Pa)
p_g	gas pressure (Pa)
p_{ga}	pressure of dry air (Pa)
p_{gwa}	pressure of moist air (Pa)
p_{gw}	water vapour partial pressure (Pa)
p_{gws}	water vapour saturation pressure (Pa)
p_w	free water pressure (Pa)
S	liquid phase volumic saturation (liquid volume/pore volume)
t	time (s)
T	temperature (K)
$\mathbf{u}$	displacement vector of solid matrix (m)
$\mathbf{v}_{gwa}$	velocity of moist air (m s^{-1})
$\mathbf{v}_l$	velocity of liquid phase (m s^{-1})
$\mathbf{v}_b$	velocity of physically bound adsorbed water (m s^{-1})
$\mathbf{v}^d_{ga\text{-}gw}$	relative average diffusion velocity of dry air in water vapour (m s^{-1})
$\mathbf{v}^d_{gw\text{-}ga}$	relative average diffusion velocity of water vapour in dry air (m s^{-1})
$\mathbf{v}_s$	velocity of solid phase (m s^{-1})
w	free water

Biot constant

$\alpha-\beta$	exothermic inversion during heating up at 573°C
α_c	convective heat transfer coefficient (W m^{-2} K^{-1})
β_c	convective mass transfer coefficient (m s^{-1})
$\beta-\alpha$	endothermic inversion during heating down at 573°C
Δh_{phase}	enthalpy of vaporisation per unit mass (J kg^{-1})
$\Delta \boldsymbol{m}_{hydr}$	mass source term related to hydration–dehydration process (kg m^{-3} s^{-1})
$\varepsilon^{\sigma,T,m}_{t,tot}$	total strain
$\varepsilon^{\sigma,T,m}_{0,el}$	elastic strain
$\varepsilon^{0,T,m}_{0,th}$	thermal strain
$\varepsilon^{0,T,m}_{0,sh}$	shrinkage strain
$\varepsilon^{\sigma,T,m}_{t,cr}$	creep strain
$\varepsilon^{\sigma,T,m}_{0,crack}$	crack strain

* Department of Civil and Environmental Engineering, Imperial College, University of London, London, UK.
† Department of Construction and Transportation Engineering, University of Padua, Padua, Italy.

(MCR 875) Paper received 26 June 2000; last revised 10 October 2001; accepted 16 November 2001

0024-9831 © 2002 *Thomas Telford Ltd*

$\varepsilon_{0,plas}^{\sigma,T,m}$	plastic strain
$\varepsilon_{0,auto}^{\sigma,T,m}$	autogeneous strain
λ_{eff}	effective thermal conductivity of concrete (W m^{-1} K^{-1})
ρ	apparent density of concrete (kg m^{-3})
ρ_{ga}	dry air phase density (kg m^{-3})
ρ_{gw}	water vapour density (kg m^{-3})
ρ_{gwa}	mass concentration of water vapour in dry air phase (density of moist air) (kg m^{-3})
ρ_s	solid phase density (kg m^{-3})
ρ_w	free water density (kg m^{-3})
ϕ	total porosity (pore volume/total volume)
ϕ_{hydr}	part of porosity resulting from hydration–dehydration of concrete (pore volume/total volume)
$\boldsymbol{\sigma}$	Cauchy stress tensor (Pa)

$\nabla = \frac{\partial}{\partial \boldsymbol{x}_k}\boldsymbol{i}_k$, Nabla operator, where $\boldsymbol{i}_k$ is versor of the x_k axis (m^{-1})

Introduction

This article presents a global view of the HITECO model developed for the prediction of the thermal, hydral and mechanical response of concrete as well as high performance (HPC) and ultra-high performance concretes (UHPC) at high temperature. The main applications are fire and nuclear reactors, but also can include any Portland cement based concrete structure exposed to high temperatures.

The majority of software dedicated to modelling the effect of high temperature on concrete can be classed as thermo-mechanical. A typical example is the programme FIREXPO also developed as part of the HITECO project, Khoury *et al.*[1] Most of these essentially consist of two separate thermal and mechanical programs interfaced so that the temperature field output of the thermal program is input into the mechanical program at every time step to produce the resulting strains and stresses. The thermal and mechanical programs are not normally coupled (i.e. interactive). In other words, if the structure develops cracks that influence the heat flow then that is not reflected in the thermal analysis. Such programs are capable of predicting reasonably accurately the overall deflections of beams and columns exposed to fire, although discrepancies between experiment and model appear at the lower temperatures of 100–200°C, because the influence of evaporable moisture cannot be properly incorporated. For such applications, the relatively simple thermo-mechanical models offer a reasonably accurate and cost effective solution of predicting, for example, fire resistance of beams and columns in terms of total deformations after one or two hours of exposure to fire.

However, thermo-mechanical models are unable to predict phenomena related to moisture flow and the development of pore pressures during heating. Two important examples are explosive spalling of concrete in fire and the moisture state of nuclear reactor concrete.

Explosive spalling can result in significant loss of section leading to reduction in load-bearing capacity. Up to 75% of the concrete segment thickness was lost in multiple layered explosive spalling in the 1994 Great Belt tunnel fire. In the 1996 Channel Tunnel fire, up to 100% of the segment spalled off explosively. The compressive strength of the high performance concretes used in these tunnels exceeded 100 N/mm^2 at the time of the fire. High performance concrete has a higher tendency to experience explosive spalling than normal strength concrete owing to its denser and less porous structure. This results in greater pore pressure during heating. The spalling problem in high performance concrete (HPC) and ultra high performance concrete (UHPC) prompted the HITECO research programme that is dedicated to the study of HPC and UHPC at high temperatures.

Another example is nuclear reactor concrete in which moisture slows down and captures nuclear radiation emitted from the reactor core (e.g. neutrons), thus helping the concrete to act as a biological shield. This applies to both the prestressed concrete reactor pressure vessels (PCRVs) used in gas cooled reactors (e.g. Advanced Gas Cooled Reactors (AGR)) and to unprestressed reactor biological shields. It is important that the moisture state of the reactor concrete is known under both service and accident conditions to ensure the maintenance of their biological shielding capability.

Where the moisture state of concrete is important, a model with a hydral component is necessary. Hitherto, the very few such models developed to date, consider the different fluid phases in concrete to be a single phase smeared fluid.[2] The HITECO model reported in this article considers fluid in concrete to comprise liquid and gas phases. Furthermore, the model is a fully-coupled (i.e. interactive) multi-phase hydro-thermal-mechanical model for concrete (including high performance concrete) at high temperature. Another significant departure from previous trends is that the model is not only driven by mathematical rigour but also by realistic understanding of the behaviour of the material, which in concrete is complex both chemically and physically, especially at high temperature. The input material behavioural data are, therefore experimental—performed as part of this programme of work.

This article presents the overall structure of the HITECO model by describing the three key components of the model, namely

(*a*) *The physical model* describing the concrete multiphase physico-chemical structure of the concrete as modelled. This includes description of state variables, transport processes, phase changes and mechanical processes.

(*b*) *The mathematical model* in four components (general laws of conservation, constitutive relationships, thermodynamic equations and the initial and boundary conditions).
(*c*) *The numerical solution* employed including the space and time discretisation solutions as well as the algorithmic treatment of non-linearities.

In all the three foregoing cases, the first section begins with a listing of the assumptions made so that it is clear to the reader what simplifications were introduced and how the model was constructed. Furthermore, given the complexity of this model, its mathematical treatment in the traditional manner can be cumbersome consisting of a very large number of equations and terms. It was, therefore, decided to present here only the main equations. The structure of the equations and the relationships between them are also described in a flow chart/table form thus providing the overall global view. The causes and effects are also described textually so that the article could be understood by the general scientist/engineer and not just by modelling experts; the emphasis being throughout on clarity and logical development of the problem. The discussion highlights the advances made by this article as well as its limitations and potential for future development. The article concludes with example outputs from the model demonstrating its capabilities graphically. Details of how the individual thermal-hydral-mechanical properties were formulated into the model are beyond the scope of this article and will be presented in future articles.

The theoretical model used here is based on the works of Whitaker,[3] Bear,[4,5] Bear and Bachmat,[6–8] Hassanizadeh and Gray,[9–11] and Schrefler[12] for porous media at room temperature, with modification for concrete at moderately high temperatures by Baggio *et al.*[13] and for high temperatures by Gawin *et al.*[14]

Further upgrading by the present authors was introduced as part of the HITECO project for phase changes (e.g. additional phase changes), creep effects (e.g. transient creep), tensile properties (e.g. stress–strain at high temperature in direct tension), pore structure, sorption/desorption, permeability and damage in concrete. In addition, new experimental thermal-hydral-mechanical data were input for the first time by the present authors for HPC and UHPC including their related mathematical and numerical treatments. Importantly, this article introduces for the first time the mechanism of modelling the explosive spalling of concrete in fire. The model presented by the present authors offers, overall, significant advances on the previous concrete model for high temperature of Bazant and Thonguthai[15] and which is also described in a recent book by Bazant and Kaplan.[2]

HITECO research programme

The BRITE-EURAM HITECO (i.e. high temperature concrete) research programme initiated in January 1996 was funded by the European Commission under contract BRPR-CT95-0065. With a budget of 3·6 million Euro and technical contributions from 10 leading organisations in seven European countries (Denmark, Finland, France, Germany, Italy, Spain, the UK), the project was probably one of the largest and most comprehensive research programmes into the effect of high temperature on concrete and high performance concrete.

The development of HPC and UHPC opens new possibilities for the design of concrete structures, both for high rise buildings and more slender sections in concrete structures such as bridges. Knowledge of the behaviour of these concretes at high temperatures is, however, limited. The HITECO programme was, therefore, initiated to improve understanding of the behaviour of HPCs and UHPCs in situations involving high temperatures—such as fire and nuclear reactors. To address this issue, materials research was undertaken at both the micro-structural and phenomenological levels for a wide range of materials with compressive strengths ranging from 60 MPa to 173 MPa (Table 1). The properties investigated extend beyond the mechanical properties and include also thermal and hydral properties. The materials

Table 1. Information on four HPC and two UHPC concretes

Parameter	Concrete					
	C-60	C-60-SF	C70	C90-SF	CRC	RPC-AF
Manufacturer	Bouygues	Aalborg	Addtek	Addtek	Aalborg	Bouygues
Classification	HPC	HPC	HPC	HPC	UHPC	UHPC
28 day compr. str. (MPa)	67	65	85	102	142	173
Silica-fume	No	Yes	No	Yes	Yes	Yes
Fly-ash	No	Yes	No	No	No	No
AEA	No	Yes	No	No	No	No
Aggr. size	Normal	Normal	Normal	Normal	Sand	Sand
W/blend	0·36	0·42	0·32	0·32	0·16	0·14
pp fibres	No	No	No	No	No	Yes
Steel fibres	No	No	No	No	Yes	Yes
Heat treatment	No	No	No	No	Yes	Yes

characterisation constitutes the first stage of the test programme leading towards the study of the behaviour of structures (made with HPC/UHPC materials) by means of large-scale testing of elements and prototype structures exposed to ISO Standard (similar to BS476) and hydro-carbon time–temperature fires regimes, as well as to the slower heating conditions relevant to nuclear reactors.

A major factor inhibiting the use of HPC is its increased tendency to experience explosive spalling in fires owing to its denser structure that does not readily allow the escape of moisture during heating. High pore pressures, therefore, develop within the HPC structure contributing to a greater probability of explosive spalling when compared with normal strength concrete. Experimental/theoretical investigations have, therefore, been carried out to help better understand this phenomenon. A key contribution from the HITECO programme in this important area of study is the development of the HITECOSP (High Temperature Concrete Spalling) software capable of predicting—in a fully integrated fashion—the thermal, hydral and structural response of concrete structures exposed to heating. The materials test programmes of the different laboratories have been designed so that the test outputs provided data appropriate as input values into the software, while the large scale testing of prototype structures provided the opportunity to validate the program.

Physical model

Concrete is here considered to be a multiphase medium where the voids of the solid skeleton could be filled with various combinations of liquid- and gas-phases (Fig. 1).

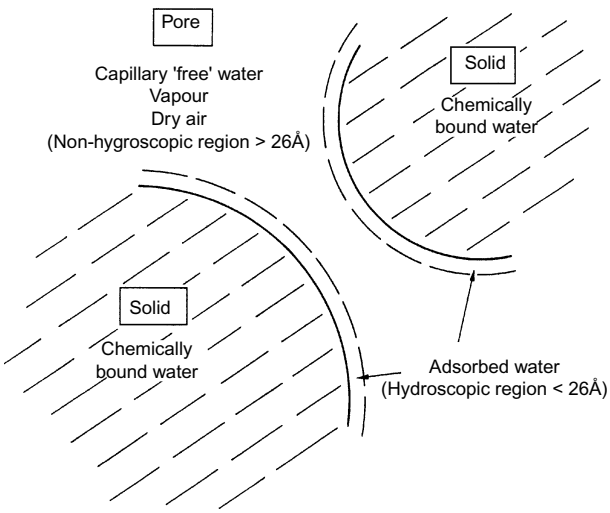

Fig. 1. Different forms of fluids considered in the physical concrete model

General assumptions

The general assumptions for the physical model are listed as follows.

(*a*) Porous medium: concrete is treated as a porous medium (e.g. a solid skeleton with fluids filling pore space containing dry air, vapour, moist air, capillary water and physically adsorbed water). The chemically bound water is considered to be part of the solid skeleton until it is released on heating.

(*b*) Level of investigation: at the macro-level, plain concrete can be idealised into a porous continuum where all the constituents of concrete (solids, voids and fluids) are 'smeared' inside a reference element volume (REV). At the meso-level, concrete is represented by aggregate, bond region and paste/mortar with separate characteristics. Therefore, at the meso-level there exists three REVs, all of which could also be porous media depending upon their characteristics (e.g. some aggregates may be considered non-porous). At the micro-level (optical), the concrete is represented by three types of solid (aggregate, solid skeleton paste in two phases (bond region and matrix)) and separate pores through which fluids flow. The current stage of this article treats concrete at the macro-level, but an extension into the meso-level analysis is within the scope of the model. The addition of reinforcement and prestressing is also a straightforward extension.

(*c*) Full coupling: at the macro level, the solid and fluid constituents in a REV are fully interacting.

(*d*) Space averaging: all transport phenomena of the solid and fluid constituents occur inside the macro-level smeared REV.

(*e*) Three-dimensional: the physical model and related mathematical equations of conservation, and thermodynamics are fully three-dimensional. Three dimensionality of the constitutive relations requires the availability of materials properties in three dimensions, requiring changes in the model to accommodate the third dimension. The numerical treatment (e.g. discretised equations) is also fully three-dimensional. However, at the current stage of development, the finite element software only performs plane stress, plane strain and axisymmetric analysis. An extension to full three dimensionality is still straightforward requiring only an extension of matrices and vectors. However, for very large structures, parallel computing is advantageous to speed-up the three dimensional calculations. Overall, extension to three dimensionality is a relatively simple exercise from the numerical and finite element perspectives and the key difficulty lies in the appropriate use of three-dimensional data in the constitutive equations.

(*f*) Thermodynamic equilibrium: all the solid and fluid

constituents at a given time in the REV are in thermodynamic equilibrium (i.e. the temperature is equal for all the constituents).

(*g*) Small strains: the strains are considered for the solid skeleton as infinitesimal in the first order.

(*h*) Strain components: the strain components of the solid skeleton are the: elasto-damage strain, plastic, creep, thermal, shrinkage, cracking and autogeneous (due to chemical phase changes such as hydration). They are assumed to obey the superposition theory of strains.

(*i*) Damage: microcracking effects are taken into account by means of damage. Damage is here represented by either a reduction in the damaged area (reduced to zero for total damage) or a reduction in the value of the elastic modulus. The damage parameter $1 \geqslant D \geqslant 0$ equals 1 for fully damaged material and 0 for an undamaged material.

(*j*) Temperature–pressure dependency: all the material properties are assumed to be temperature and pressure dependent in the whole temperature range of interest from ambient (≈ 20°C) up to 1000°C. The water modelling is valid up to the critical point of water at 374·15°C at which point, and higher temperatures, capillary water does not exist—only vapour.

Liquid, gas and solid phases

The liquid phases (i.e. l) in the model consist of three phases (Fig. 1)

(*a*) Capillary water (or free water, $\mathrm{l} = w$), which is present outside the 'hygroscopic region' for $1 > S > 0$

(*b*) Physically bound 'adsorbed' water ($\mathrm{l} = b$) which is present inside the hygroscopic region (< 26Å) within the influence of solid surface forces

(*c*) Chemically bound water of hydration (e.g. CSH, CH) which is part of the solid skeleton until it is released at certain high temperatures and then is considered in the equations as an increase in mass of the vapour phase. Mass change from hydration/dehydration is considered in the 'phase' change terms and in the rate of change of hydration/dehydration mass (note that $\mathrm{C} = \mathrm{CaO}$, $\mathrm{S} = \mathrm{SiO_2}$, $\mathrm{H} = \mathrm{H_2O}$).

When all the free water has been removed ($S = 0$), and the solid skeleton remains fully saturated with adsorbed water, this point is known as the solid saturation point (SSP). At this stage only the adsorbed and chemically bound water are present in the concrete.[15]

The gas phases (i.e. g) in the model consist of three phases (Fig. 1)

(*a*) dry air '*ga*' (non-condensable constituent)

(*b*) water vapour '*gw*' (condensable gas)

(*c*) mixture of the two '*gwa*' (i.e. moist air)

and are assumed to behave as ideal gases.

The solid phase (i.e. *s*) is that of the solid skeleton of the matrix (Fig. 1) which contains chemically bound water but is considered as a 'dry' phase. Chemically bound water starts to be released on heating above 80°C in the unsealed condition and continues to be released as a function of increasing temperature. The release of this water reduces the mass of the solid skeleton. The reverse is true for hydration when the mass of the solid skeleton is increased.

State variables

The state variables (Table 2) have been selected for the model as the essential main variables. They are the hydral (p_{gwa}, p_c), thermal (T) and mechanical ($\mathbf{u}$) variables. They can also be applied as boundary conditions. Other derived 'secondary' state variables described in Table 3 used in the formulations relate to the main state variable via thermodynamic relationships. Both the main and secondary state variables become outputs of the model (i.e. software) over the whole space and time domain.

Mass conservation

Mass conservation applies to the conservation of solid, liquid and gas phases. Any phase changes (e.g. evaporation or solid dehydration) are also incorporated in the model. The individual constituents of each phase in the concrete model are presented in Table 4.

Transport mechanisms

Transport mechanisms in the concrete model comprise the transport of heat, fluid and solid. These are summarised into components in Table 5 together with respective driving mechanisms for the fluid and solid phases. Temperature causes changes in all three transport components (heat, solid, fluid). Temperature gradients induce heat flow down the gradient, but it also drives moisture into the concrete as well as outwards (if the surface is unsealed). This induces a moisture

Table 2. Chosen main state variables in concrete

State variable	Meaning
p_{gwa}	Moist air pressure (see Dalton's law in Fig. 21)
p_c	Capillary pressure
T	Temperature
$\mathbf{u}$	Displacement vector of the solid matrix

Table 3. Derived (or secondary) state variables in concrete

State variable	Meaning
p_{ga}	Dry air pressure (see Dalton's law in Fig. 21)
p_{gw}	Water vapour pressure (see Dalton's law in Fig. 21)
p_{gws}	Saturation vapour pressure
p_w	Free water pressure ($= p_{gwa} - p_c$)
RH	Relative humidity

Table 4. Constitutents of three phases in the concrete model

Phases	Constituent
Solid phase	Solid matrix (skeleton)
Liquid phases	Capillary 'free' water Physically bound 'adsorbed' water Chemically bound water
Gas phases	Dry air Water vapour Moist air

gradient and pore pressure gradients thus contributing to diffusional and Darcian flows respectively. The solid component experiences dilatation as well as cracking that influences the structure within which the fluids flow. Changes in the pore structure (volume and distribution) are caused by hydration/dehydration processes, dilation, loss of moisture, etc. Therefore, the most appropriate modelling approach—adopted in this article—is one that fully couples all three thermal, hydral and mechanical components that are essentially interactive.

Phase changes (physico-chemical)

Phase changes take place that can be physical or chemical in nature. Phase changes in concrete are, for the first time, incorporated directly in the transport mechanism of the concrete model (Table 6). For Portland cement-based concretes, they are: CSH and CH dehydration/hydration, evaporation/condensation, sorption/desorption, physical phase changes (e.g. $\alpha-\beta$ transformation of quartz at 573°C), and decarbonation of calcium carbonate above 650°C.

Hydration (chemical). Hydration takes place at room temperature and the process increases with temperature in the presence of moisture up to 80°C or more resulting in an increase in the mass of the solid skeleton. It should be noted that if cement paste is heated above 100°C in the presence of moisture under hydrothermic conditions, depending upon the C/S ratio, a chemical transformation of tobermorite will take place to produce $C_2SH(A)$ hydrate (Fig. 2) which is a weak, porous and crystalline material. Further chemical changes take place at higher temperatures under hydrothermal conditions. In addition, reactive silica in the concrete (aggregate or cement replacement) would also react beneficially with water and CH to produce CSH phases (Fig. 3). The use of cement replacements such as silica fume, PFA or slag reduces the amount of CH produced upon hydration (Fig. 5) and increases the amount of CSH produced thus creating a stronger and less permeable material. These changes have not been modelled in this version but may be modelled in future versions of the software.

Dehydration (chemical). Dehydration (i.e. release of chemically bound water) from the CSH becomes significant above about 110°C (Fig. 4), while the dehydration of the calcium hydroxide (Fig. 5) takes place at about 500°C producing CaO and H_2O. Both produce a reduction in the solid skeleton mass of the cement paste. However, the strength of concrete is more related to the CSH than the CH. The release of chemically bound water contributes moisture to the gas phase and contributes to vapour pressure that becomes significant in high performance concrete with low porosity and low permeability and could contribute to explosive spalling. The temperature at which dehydrations occur depends upon the activation energy E_a of the chemical. The CSH is a complex chemical with a range of activation energies for its constituents.

Evaporation (physical). Evaporation of water from concrete increases with temperature above 100°C, de-

Table 5. Transport mechanisms in the concrete model

Transported component			Mechanism
Heat			Heat transport by conduction and advection within the porous medium Heat transport by convection and radiation at external surfaces
Solid			Mechanical displacement (thermo-hydro-mechanical loading)
Fluid	Liquid	Capillary water Adsorbed water Chemically bound water	(= free water) Darcian flow (capillary pressure gradient) Diffusional Fick's flow (adsorbed water saturation gradient) no fluid transport (part of the solid matrix)
	Gas	Dry air	Darcian flow (moist air pressure gradient) and diffusional Fick's flow (dry air concentration gradient)
		Water vapour	Darcian flow (moist air pressure gradient) and diffusional Fick's flow (water vapour concentration gradient which is influenced by the Knudsen effect in narrow pore)*
		Moist air	Darcian flow (moist air pressure gradient)

* During diffusion of vapour in very narrow pores (< 100Å), the number of collisions of water molecules with the solid matrix is non-negligible compared with the number of collisions with air molecules, thus also Knudsen effects are of importance. This causes a decrease in vapour diffusion flow and is modelled in this work.

Table 6. Brief description of some phase changes in concrete

Phases	Process	Energy	Phase change process
Dehydration Hydration	Chemical	Loss Gain	Solid matrix (CSH or CH) ⇒ water − energy + matter (C or C_yS) water + matter (C or C_xS) ⇒ solid matrix (CSH or CH) + energy
Evaporation Condensation	Physical	Loss Gain	Capilllary water ⇒ water vapour − energy Water vapour ⇒ water + energy
Desorption Sorption	Physical	Loss Gain	Physically adsorbed water ⇒ water vapour − energy Water vapour ⇒ physically adsorbed water + energy
Decarbonation*† Carbonation	Chemical	Loss Gain	Calcium carbonate ⇒ CO_2 − energy CO_2 ⇒ Calcium carbonate + energy
$\alpha-\beta$ inversion*‡ $\beta-\alpha$ inversion	Physical	Loss Gain	Endothermic during heating up at 573°C with expansion Exothermic during heating down at 573°C with contraction

* to be incorporated in a future version of the model
† occurs in both carbonate aggregates and cement paste above 600°C
‡ occurs in the quartz aggregates and sands

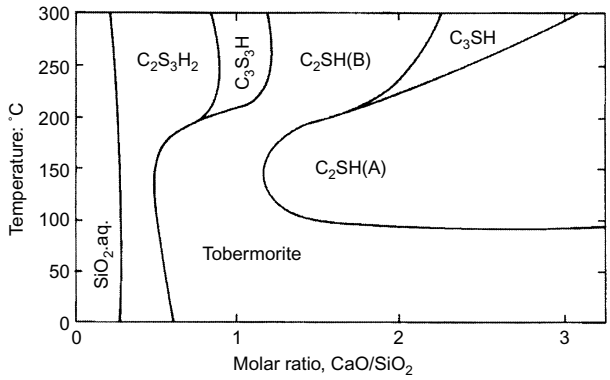

Fig. 2. Chemical transformations/hydration in moist cement paste as a function of temperature and C/S ratio[16]

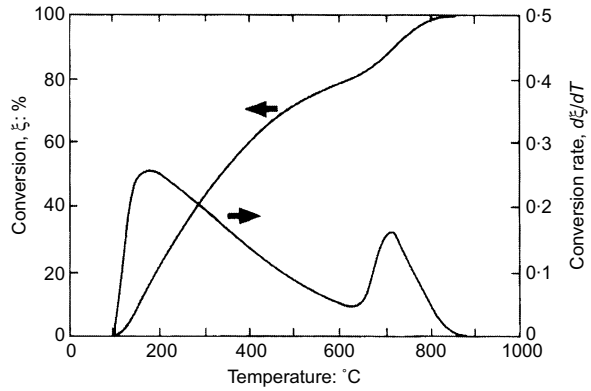

Fig. 4. Degree and rate of conversion (dehydration) of tobermorite (CSH) in an idealised cement paste[18]

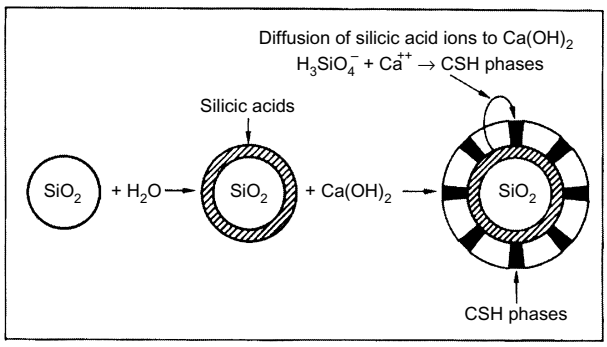

Fig. 3. Reaction of silica with water and CH to produce CSH phases[17]

pending upon the pressure. The loss of capillary water (Fig. 1) does not significantly influence the mechanical properties of the cement paste (e.g. shrinkage) but the loss of physically bound water has a major influence on the mechanical properties. For a small element of concrete the capillary water would evaporate completely by 100°C. However, for relatively large elements, the evaporation from the surface, especially for dense concretes, may not be rapid enough to release all the capillary water from the body by 100°C and some water may in fact be driven down the temperature gradient into the material. Therefore, capillary water may remain within the body for a period during which temperatures exceed 100°C, particularly for dense concrete, thus contributing to the chemical hydrothermal changes mentioned above and to explosive spalling. No free water is possible above the critical point for water (374·14°C) at which point capillary water and capillary pressure disappear while only some physically and chemically bound water, water vapour (and pressure) and dry air exist above this temperature.

$\alpha-\beta$ transformation of quartz (physical). The $\alpha-\beta$ transformation of quartz occurs at 573°C in aggregates and sands containing quartz (Fig. 6). This is an endothermic reaction during heating, and exothermic during cooling when the transformation is reversed.

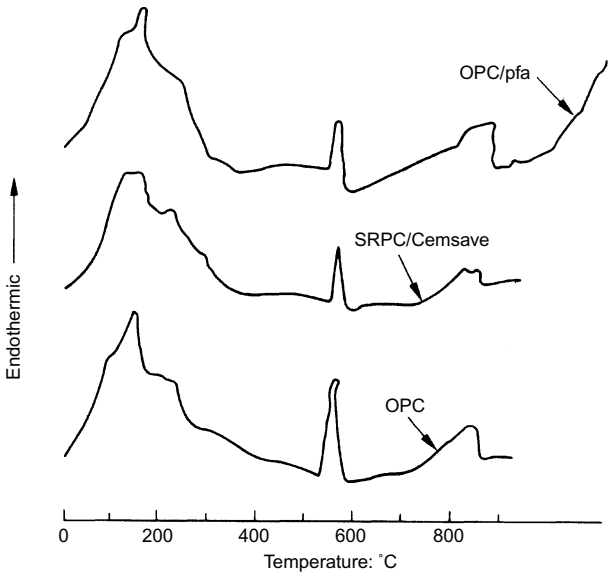

Fig. 5. Differential thermal analysis (DTA) of three cement pastes (10°C/min in N_2) showing an endothermic peak at about 550°C from dehydration of CH. Amount of initial CH in the cement paste is reduced when cement replacements (pfa, slag, silica fume) are used[19]

Decarbonation (chemical). Decarbonation (Fig. 6) occurs at temperatures above 650°C whenever $CaCO_3$ is present in the aggregate (e.g. limestone and carbonate aggregates). This produces lime (CaO) and carbon dioxide (CO_2).

Rehydration of lime (chemical). On cooling, the CaO produced from the dehydration of CH and decarbonation of the $CaCO_3$ absorbs water and rehydrates into $Ca(OH)_2$ with a corresponding 40% increase in volume. This is modelled in the present version of the model.

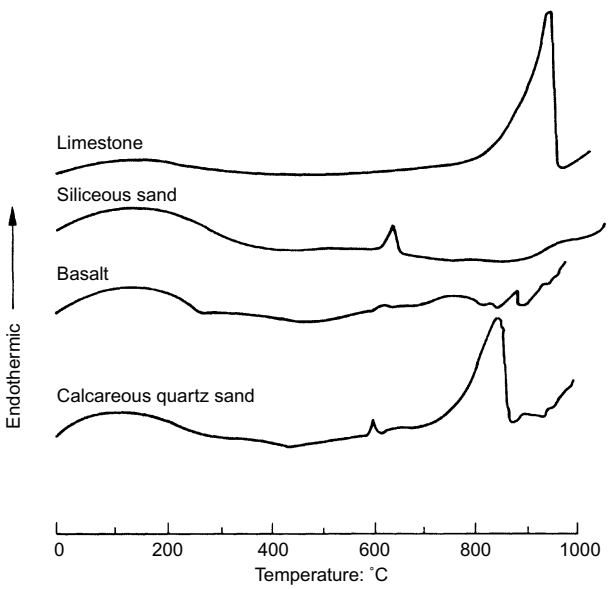

Fig. 6. Differential thermal analysis (DTA) of four aggregates (10°C/min in N_2) showing an endothermic peak at about 575°C from $\alpha-\beta$ transformation of quartz and large peaks for dissociation of $CaCO_3$ at higher temperatures[19]

Summary of phase changes. All the phase changes are strongly influenced by temperature, and are strictly thermodynamically not fully reversible, although reversibility is often assumed in mathematical modelling.

Mechanical properties

This section presents the key features of the mechanical behaviour of concrete at high temperature that provide the necessary input for numerical modelling. Modelling the complex nature of the mechanical behaviour of concrete at high temperature benefits from up-to-date knowledge of computational elastic, creep, damage, plastic and fracture mechanics. Such a model will need the input of realistic materials properties data. Ignoring important factors in the model, such as the influence of load upon the strain behaviour of concrete during first heating could produce meaningless results.

Properties related to the stress–strain relation. The stress–strain relation is determined by short-term loading of concrete at constant temperature to failure. Therefore, to determine the stress–strain relation at, for example, 300°C the specimen needs to be heated first to 300°C and then maintained at this temperature for an hour (to equalise temperatures within it), and then the test would be performed. The key feature in this test is whether the specimen is heated under load or without load. The results could be radically different as shown in Figs 7 and 8. This feature has not been fully appreciated by scientists and engineers in the past. The various elements of the stress–strain relation at high temperatures are described as follows.

(*a*) The ascending branch comprises essentially three components: (i) an elastic recoverable strain component that is temperature dependent and is influenced strongly by the load level during initial heating to the test temperature (Figs 7 and 8); (ii) an irrecoverable plastic strain component; and (iii) a time-dependent creep component which is normally small at room temperature but can be significant at high temperatures, particularly above 550°C (Fig. 20). For high strength concrete (e.g. C70, Fig. 7), the ascending branch at room temperature is linear for stress levels up to 50% of the maximum stress or higher indicating that irrecoverable components of strain are small. The effect of high temperature is to reduce the slope of the curve and render it non-linear except when the material is heated under load in which case it remains closer to the original slope and linear. For higher

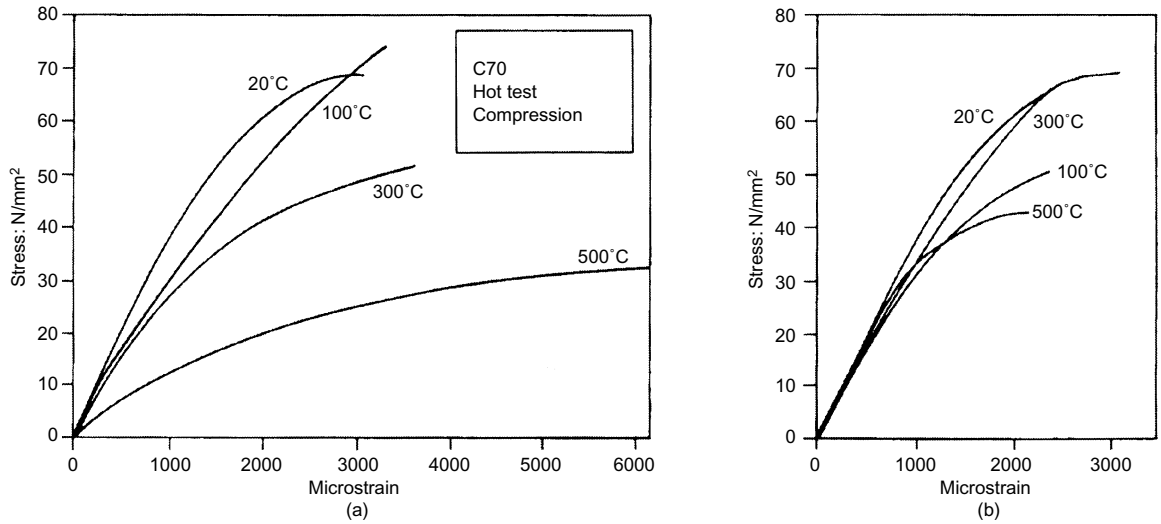

Fig. 7. Effect of temperature (and load level during heating-up at 2°C/min as a percentage of strength prior to heating) upon the stress–strain relation in uniaxial compression measured at temperature in the 'hot' state for unsealed C70 HITECO concrete containing thermally stable Gabbro Finnish aggregate. The tests were conducted at constant stress rate so the descending branch is not produced: (a) 0% load; (b) 20% load[20]

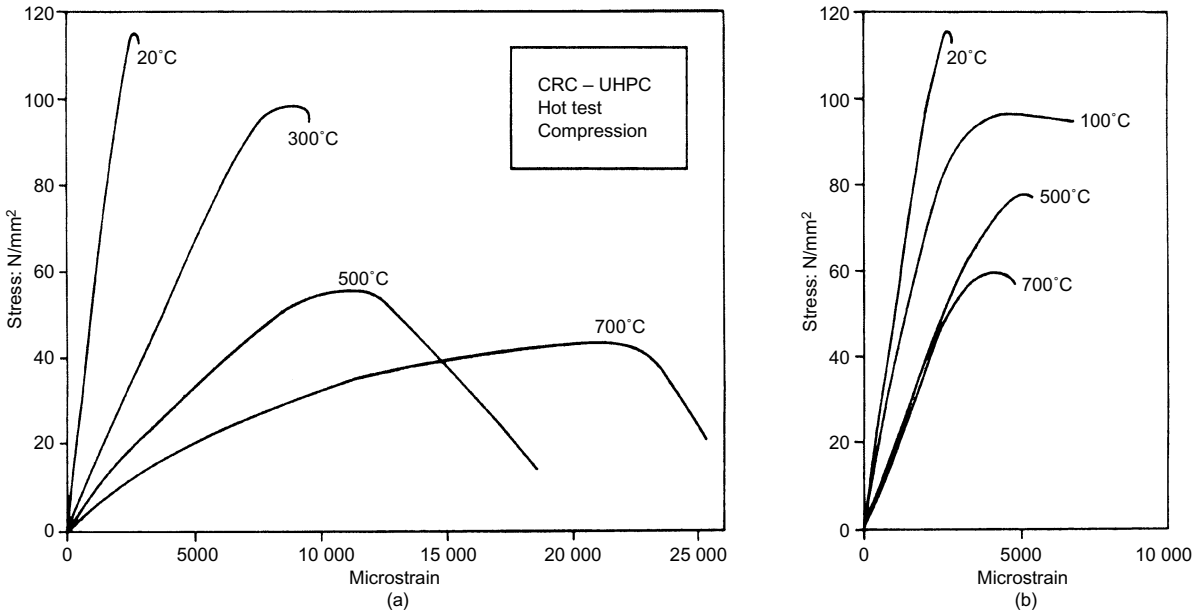

Fig. 8. Effect of temperature (and load level during heating-up at 2°C/min as a percentage of strength prior to heating) upon the stress–strain relation in uniaxial compression measured at constant temperature in the 'hot' state for unsealed CRC HITECO ultra-high performance concrete. The tests were conducted at constant deformation rate allowing the descending branch to be measured: (a) 0% load; (b) 20% load[21]

strength concrete (e.g. ultra-high performance concrete $> 100\text{N/mm}^2$—Fig. 8) the linearity extends up to about 80% of the maximum stress and is not significantly affected by temperature except for the unloaded condition tested at 500–700°C. These high strength materials are also brittle possessing a small descending branch except when the concrete is heated without load and tested at 500–700°C (Fig. 8), thus indicating a softening of the material at those temperatures. The stress–strain relation in *direct* tension at high temperature (i.e. in the 'hot' state) was tested for the first time ever at Imperial College, UK in collaboration with Milan Politecnico, Italy (as part of the HITECO project) and the results, shown in Fig. 14 for the C90 HITECO concrete, are input into this model.

(*b*) The static modulus of elasticity is determined in different ways including the initial tangent modulus as well as the secant modulus. A typical feature of this property at high temperatures is that it normally reduces more with increase in temperature than the strength when heated without load, but 'benefits' from heating under load more that the strength (Fig. 9). The dynamic modulus of elasticity is measured without the applied load and because it excludes creep and cracking it is always greater than the static modulus and is closer to the tangent than the secant modulus. The results of the stress analysis of heated concrete could be influenced by the 'type' of elastic modulus used. It is best to input the entire stress–strain curve (including the descending branch) in both compression and tension for the whole temperature range.

(*c*) Strength is the maximum stress attained by the specimen in both compression and in tension. In compression, it is the most investigated property of concrete at high temperature in the literature. Direct tensile strength results have never been measured before and the first results are shown in Fig. 14(b) for the C90 HITECO concrete. The important feature to emphasise is that there are huge variations in the compressive strength of concrete at high temperature (Fig. 13) depending upon: (i) the type of concrete in question which is influenced by the cement blend and aggregate used (Figs 10–12); (ii) the sealing/moisture condition (Fig. 13); (iii) the load level during heating up (Figs 9 and 12); (iv) whether the measurement is taken in the 'hot' state or 'residual' after cooling (Fig. 13); (v) rate of heating/cooling; (vi) duration at constant temperature; (vii) length of time maintained in moist conditions after cooling before the test is carried out; and (viii) number of previous thermal cycles (Fig. 13). Clearly, such varied influences present difficulties for modellers and the best approach would be to ensure that the software run applies to a specific concrete. All data must be consistent for one material to avoid inappropriate analysis. Second, it is important to consider the role of the load level during heating. The conservative approach would be to regard the 0% load level as the base case because it usually results in a greater reduction in strength with temperature than in the case of, say, the 20% load level (Figs 7–9, 12, 13), but a stress function could be introduced to incorporate this feature.

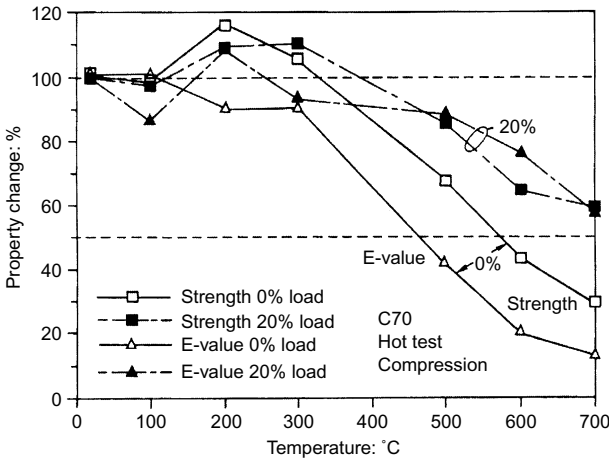

Fig. 9. Effect of temperature upon the residual (after cooling) compressive strength and elastic modulus of unsealed C70 HITECO concrete containing thermally stable Gabbro Finnish aggregate and heat cycled at 2°C/min under 0% and 20% load (expressed as a percentage of strength prior to heating)[21]

Poisson ratio. The Poisson ratio is required to determine the behaviour of the material in multidimensional problems. Measured values of this property are rare and somewhat contradictory at high temperature but they do exist and do not indicate a strong dependence upon temperature.[22]

Thermal strain. Thermal strain is strictly the strain obtained when concrete is heated without load and excludes shrinkage. However, it is normal practice to include drying shrinkage in the definition of the term 'thermal strain' because, previously, the shrinkage component that develops during the transient heating-up process has not been separated out. This has now been achieved experimentally as shown in Fig. 18. Thermal strain of concrete is most strongly influenced by the thermal strain of the aggregate (Fig. 17(a)) and to a much lesser extent by the thermal strain of the cement blend used (compare concretes B1 and B2 in Fig. 17(a) which contain the same basalt aggregate but different cement blends). The thermal strain has an important influence upon the development of stresses within heated concrete and the higher the thermal expansion of the aggregate, the greater will be the thermal stresses. These are, however, significantly relaxed during first heating by development of the load induced thermal strain (LITS) or 'transient creep'.

Load induced thermal strain ('transient creep'). The LITS is determined indirectly as the difference between the strain measured during first heating without load and that measured under load —excluding the initial elasto-plastic strain (Figs 15 and 17). LITS is, therefore, the strain that develops when concrete is heated for the first time under load and essentially comprises the creep components of 'basic' creep, drying creep and 'transitional thermal creep' (TTC) as well as changes in the elastic strain that occur during the heating process.[23] The combination of TTC and drying creep is often called 'transi-

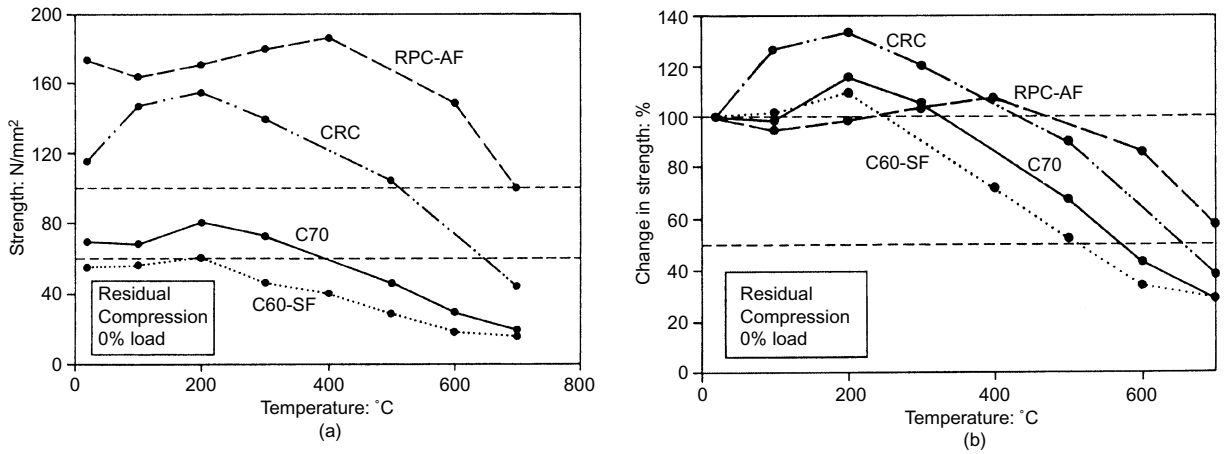

Fig. 10. Effect of temperature upon the residual (after cooling) compressive strength of two high performance concretes (C60-SF and C70) and two ultra-high performance concretes (CRC and RPC-AF) after heat cycling without load at 2°C/min: (a) actual data; (b) percentage of initial strength at 20°C[21]

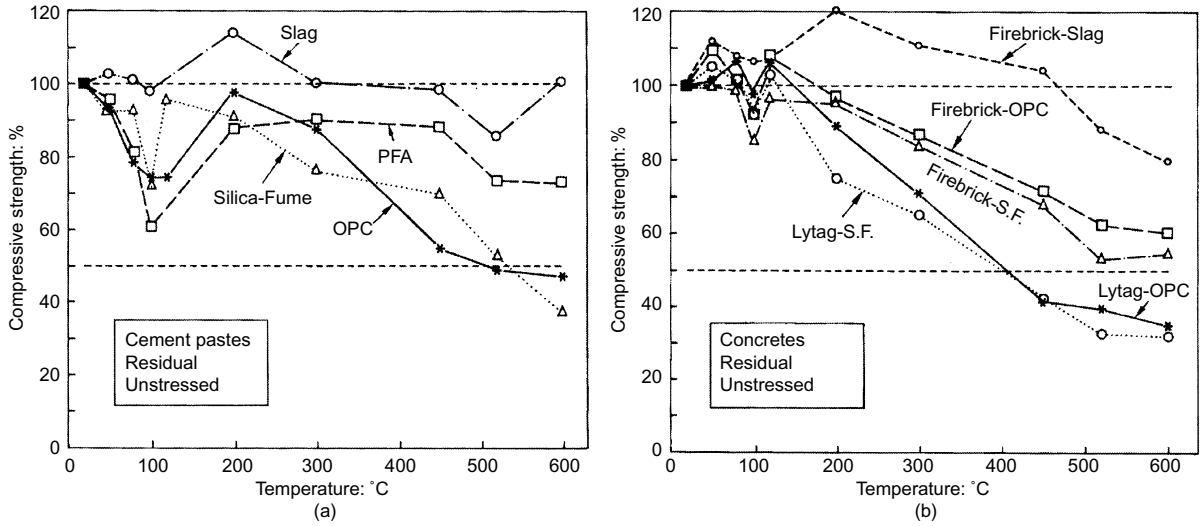

Fig. 11. Influence of: (a) type of cement; (b) type of aggregate upon the residual uniaxial compressive strength after heat cycling at 1°C/min in the unsealed condition to different temperatures without load

ent creep' and is by far the largest strain component of unsealed concrete heated to high temperatures as indicated in Fig. 16. Transient creep seems to be peculiar to concrete and occurs only during first heating to a given temperature, but not during cooling or re-heating under load. It is seated in the cement paste and is related to the complex physico-chemical transformations that occur in the CSH during first heating. Interestingly, LITS of concretes containing different aggregates are very similar despite the fact that their thermal strains are radically different (Fig. 17), providing the total aggregate by volume in concrete is also similar. It is, therefore, possible to develop a 'master' LITS curve for concrete in general which could also be normalised with respect to load if the load effect is assumed to be linear (which is not strictly true)[26] and with respect to aggregate content. This simplifies the modelling of this very important strain component. It should be emphasised that any stress analysis of heated concrete which ignores LITS (or transient creep) will provide erroneous results—a common mistake made in the past.

Cracking strain. Cracking strain is related to the development of micro- and macro-cracks during the heat cycle. It depends upon the type of concrete used, the maximum temperature attained, and the load level during the heat cycle (Fig. 19). This strain has not been included in previous models, nor has it been examined in any form in the literature. The cracking strain, now determined experimentally for the first time here, becomes significant above a 'critical' tem-

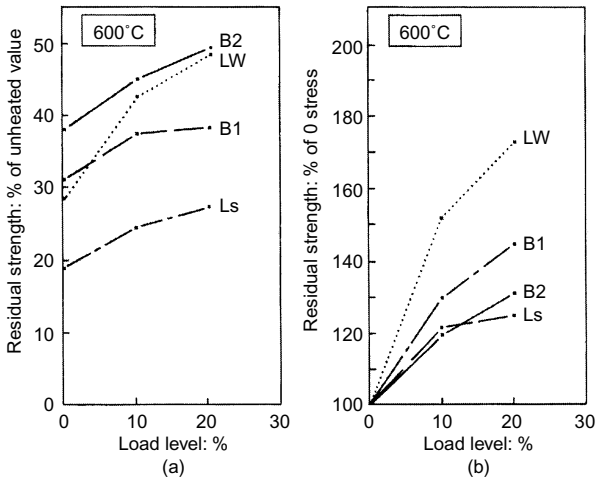

Fig. 12. Influence of load level (% of strength prior to heating) during the heat cycle (1°C/min) to 600°C upon the residual (after cooling) uniaxial compressive strength of basalt (B1 and B2), lightweight (LW) and limestone (LS) concretes[24]

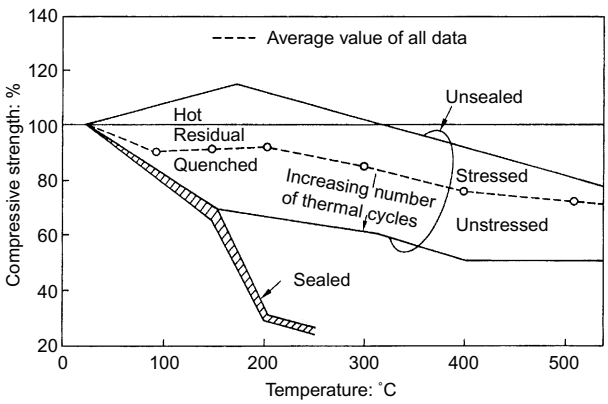

Fig. 13. Schematic diagram showing the various influences upon the compressive strength of concrete at high temperatures[25]

perature that varies according to the type of concrete and, therefore, should not be ignored.

Superposition of strain

The strain components can be modelled using the superposition theory whereby the total strain is considered to be the sum of the various strain components

$$\varepsilon_{t,tot}^{\sigma,T,m} = \varepsilon_{0,el}^{\sigma,T,m} + \varepsilon_{0,th}^{0,T,m} + \varepsilon_{0,sh}^{0,T,m} + \varepsilon_{t,cr}^{\sigma,T,m} + \varepsilon_{0,crack}^{\sigma,T,m} + \varepsilon_{0,plas}^{\sigma,T,m} + \varepsilon_{0,auto}^{\sigma,T,m} \quad (1)$$

The superposition theory has been particularly useful in the analysis of the strain components at high temperature and has been found to be applicable experimentally.[20]

Mathematical model

The mathematical model of concrete is here considered to relate to a three-dimensional domain Ω representing any porous concrete medium in Cartesian co-ordinates along with its boundary Γ. Consider a infinitesimal volume element dV, where heat and mass transfer and mechanical change occur within the body (requiring space averaging,[27] of heat, solid, dry air and water species of the medium) represented mathematically by a set of conservation equations (2–7).

Assumptions

Heat conservation equation

(*a*) Heat transport modelling in the domain: transient heat transport is here modelled by means of the Fourier's heat transport equation assuming that all the constituents of concrete are in thermodynamic equilibrium in the REV. Hence, the equation is of a parabolic type. In the steady-state temperature case it is of an elliptical type.

(*b*) Heat transport: heat conduction, heat capacity (or storage), advection (thermal diffusion) and phase changes fulfilling the first law of thermodynamics are considered in a single equation for concrete as a domain.

(*c*) Conduction: heat conduction is modelled by heat conductivity which is a non-linear function of temperature and pressure determined by experiment.

(*d*) Capacity: 'sensible' heat capacity is modelled by the sensible specific heat multiplied by the density and is also a non-linear function of temperature and pressure determined by experiment. 'Latent' heat effects are incorporated as part of the phase changes and are described by the Δh_{phase} symbol.

(*e*) Phase changes: in the current version of the model the following phase changes are incorporated: sorption–desorption, combined CSH/CH hydration–dehydration, evaporation–condensation. The hydration–dehydration of the CSH, CH and sulphoaluminate phases will also be separated so that the model can represent different types of cement. Also, the physical phase change of $\alpha-\beta$ inversion of quartz will be introduced to allow different concentrations of quartzite aggregates and sands to be modelled. The chemical change of carbonation–decarbonation will also be introduced to reflect the presence of calcium carbonates in the cement paste and in carbonate (e.g. limestone) aggregates. With these improvements it would be possible to model a wide range of concretes with different aggregates and cement pastes. All the above phase changes are non-linear functions of temperature and pressure and are determined by experiment. It should be noted that these phase changes are applicable to Portland cement based concretes and not aluminate concretes.

(*f*) Heat sources: these include 'nuclear' heating gen-

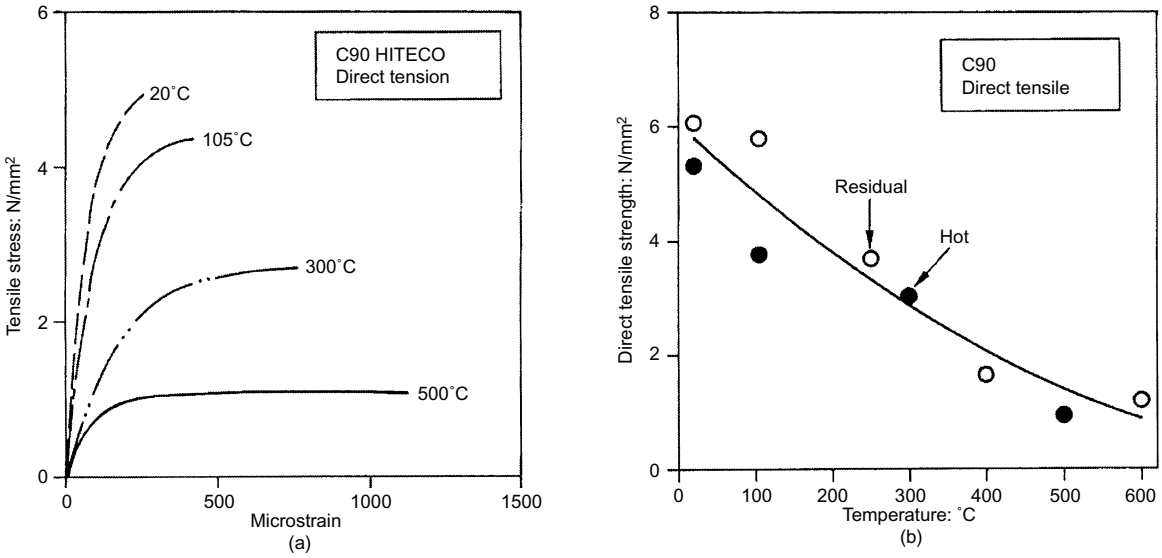

Fig. 14. Direct uniaxial tests of unsealed C90 HITECO concrete as a function of temperature: (a) stress–strain; (b) tensile strength[28,29]

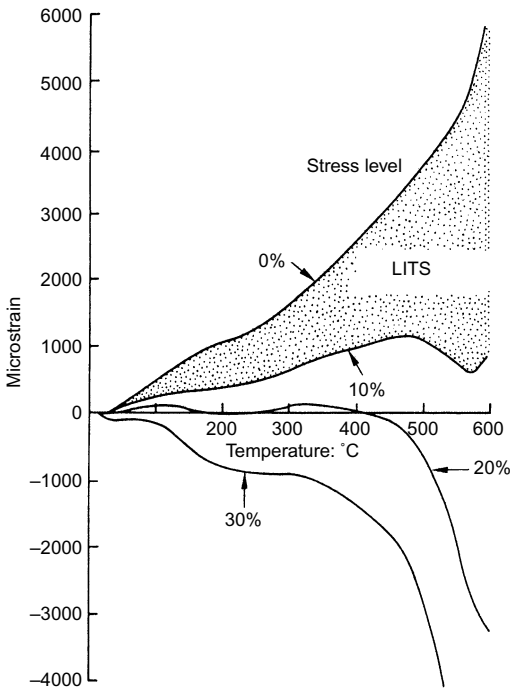

Fig. 15. Strain of unsealed basalt concrete measured during heating at 1°C/min under three uniaxial compressive load levels (% of strength prior to heating)—excluding the initial elastic strain. The load induced thermal strain (LITS) is defined as the difference between the thermal strain (0% load—including shrinkage) and the strain measured under load. LITS comprises transient creep, basic creep and changes in the elastic strain. Transient creep includes drying creep

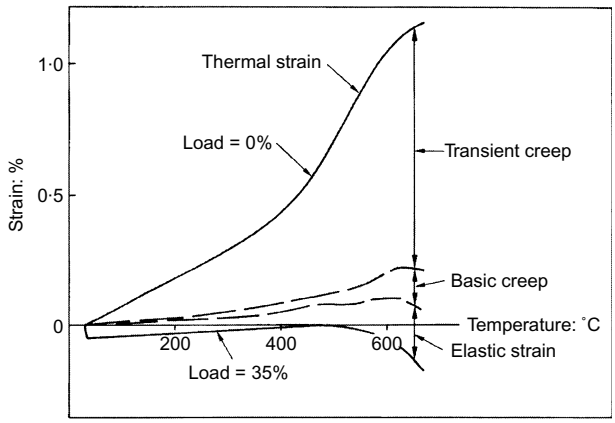

Fig. 16. Relative proportions of three load induced strains (in uniaxial compression) of concrete showing transient creep to be by far the largest component. Load level is expressed as percent of strength prior to heating[30]

erated by the slowing down and absorption of nuclear radiation. Heat can also be generated internally by electrical cables, microwaves etc.

(*g*) Boundary conditions: these can either be fixed time-dependent temperatures or heat fluxes or a combination of convection and radiation with non-linear coefficients depending upon temperature and pressures.

Solid mass conservation equation

- Solid mass conservation: solid mass conservation incorporates changes in bulk porosity of the concrete, density of the solid phase, change of mass of CSH and CH hydration–dehydration, and carbonation–decarbonation.
- Inter-relationship between parameters: solid mass conservation equation is cancelled out from the resulting system of equations providing that the three variables of bulk porosity, solid density and the combined CH/CSH hydration–dehydration change are inter-related.

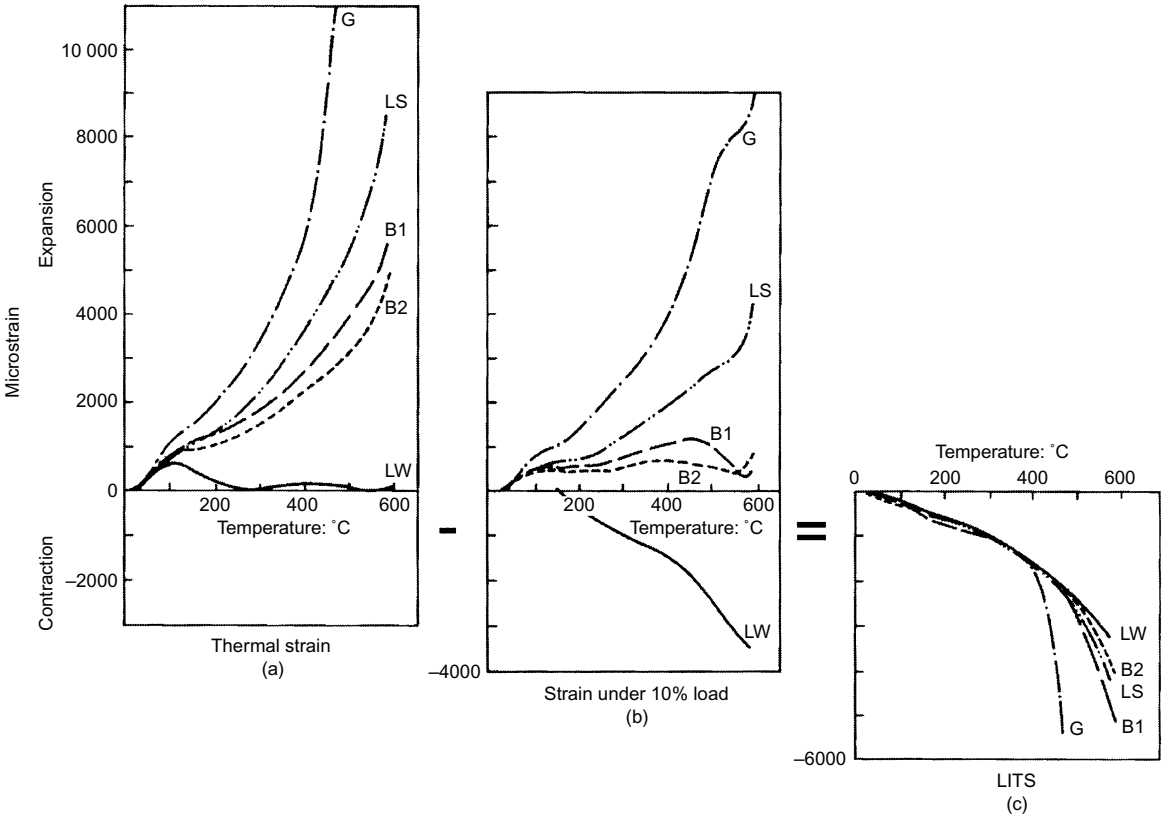

Fig. 17. Load induced thermal strains (LITS) of 5 concretes (graph c) determined as the difference in strain between the thermal strain (0% load) (graph a) and the strain measured under 10% load (graph b). Load level is expressed as percent of strength prior to heating[26]

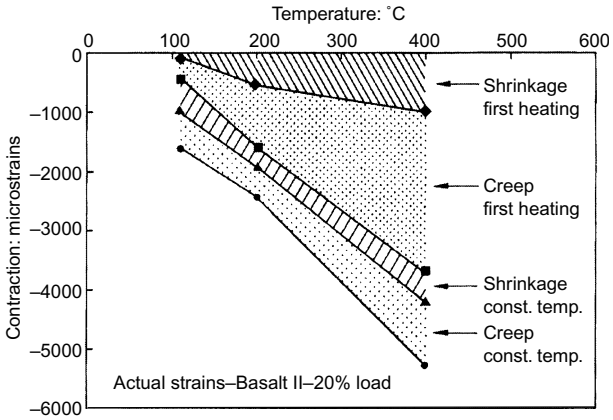

Fig. 18. Relative proportions of irrecoverable strain components that develop in unsealed basalt concrete heated at 1°C/min under 20% compressive load (relative to strength prior to heating) to constant temperature and then maintained at that temperature for 5 days[31]

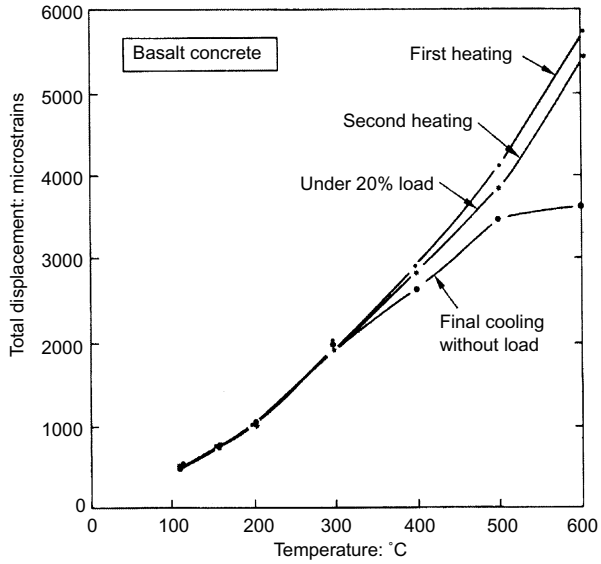

Fig. 19. Macro cracking strain component of basalt concrete determined as the difference in total strain during thermal cycling to different temperatures between the loaded and unloaded condition (in compression as percent of strength prior to heating). The critical temperature of the material is the temperature above which cracking is clearly measurable (300°C in this case)[31]

Dry air conservation equation

- Ideal gas hypothesis: dry air is assumed to behave as an ideal gas, thus obeying the Clapeyron and Dalton relationships.
- Pressure gradient driven dry air transport: the transport mechanism for dry air is that of Darcy under air pressure gradient. The key parameters are relative moist air permeability together with absolute permeability. They are non-linear functions of temperature and pressure determined by experiment.
- Concentration gradient driven dry air transport in vapour: transport of dry air inside vapour (thermo-diffusion) is modelled by diffusional Fick's law driven by dry air concentration gradient. The relevant parameter here is the diffusivity of dry air in vapour which is a function of temperature and pressure determined by experiment.
- Deformation effects: the deformation of the solid matrix allows more/less space for dry air transport. This is accounted for in the model by means of a specific term. This coupling is often disregarded by modellers.
- Storage: the storage term takes into account the capacity of the medium to accommodate dry air gain or loss. It depends on the bulk porosity and on water saturation.
- Hydration: hydration changes together with saturation allow for more space to be available for dry air gain/loss.
- Boundary conditions: these can either be fixed time-dependent dry air pressures or dry air fluxes or convective flow with non-linear coefficients depending upon temperature and pressures.

Water (liquid and vapour) conservation equation

- Ideal gas hypothesis: vapour is assumed to behave like an ideal gas, thus obeying the Clapeyron and Dalton relationships.
- Pressure gradient driven moisture transport: the transport mechanism of water and vapour is that of Darcy under air pressure gradient. The key parameters are relative water and moist air permeability together with absolute permeability. They are non-linear functions of temperature and pressure determined by experiment.
- Concentration gradient driven adsorbed water: transport of adsorbed water is modelled by diffusional Fick's law driven by the degree of saturation. The relevant parameter here is the adsorbed water diffusivity that is a function of temperature and pressure determined by experiment.
- Concentration gradient driven vapour transport in dry air: transport of vapour inside dry air (thermo-diffusion) is modelled by diffusional Fick's law driven by vapour concentration gradient. The relevant parameter here is the diffusivity of vapour in dry air which is a function of temperature and pressure determined by experiment.
- Knudsen effects: it is assumed that during diffusion of vapour in very narrow pores Knudsen effects are of importance (Table 5). The diffusivity coefficient takes into account the mean free path of water molecules in air as well as the structural coefficient pertaining to the allowable path for water molecules. The structure coefficient is a function of the temperature and saturation.
- Deformation effects: the deformation of the solid matrix allows more/less space for water and vapour transport. This is accounted for in the model by means of a specific term. This coupling is often disregarded by modellers.
- Storage: the storage term takes into account the capacity of the medium to accommodate water and vapour gain or loss. It depends on the bulk porosity and on water saturation.
- Hydration: hydration changes together with saturation allow for more space to be available for water and vapour gain/loss.
- Capillarity: two different kinds of capillary shapes are considered, spherical in the case of capillary free water and cylindrical in the case of adsorbed water. In the latter, a matric potential is assumed instead of capillary pressure to avoid additional state variables.
- Matric potential: the matric potential is a thermodynamic potential referring to the approximately 5 molecule 26Å thick adsorbed water layer which cannot be represented by capillary pressure because it has not been possible to analyse the problem at the molecular level.[33]
- Boundary conditions: these can either be fixed time-dependent vapour/capillary water pressures or fluxes or convective flows with non-linear coefficients depending upon temperature and pressures.

Momentum conservation equation

- Stresses in the solid skeleton: the total stress in the concrete is carried by both the solid skeleton and the water phases. The solid skeleton is considered to obey the Bishop's stress definition.[34] The average stresses carried by the water phases depend on saturation via average pressure. In the case of the absence of fluids (i.e. in a thermo-mechanical analysis) the solid skeleton is equal to the concrete and then the total stress and Bishop's stress are equal.
- Applied forces: the model considers applied forces at the boundary as well as forces applied inside the volume as volume forces (e.g. self weight).
- Strains in concrete: the model allows for the introduction of a range of strains such as elastic, damage, plastic, creep, shrinkage, crack and chemically induced strains. Superposition of strains is assumed as supported by experimental evidence. The influence of temperature, time and pressure upon these strains varies according to which type of strain is considered.
- Constitutive relation: the stress–strain relation for

non-saturated concrete is considered in the model to be that for the solid skeleton. In saturated concrete, the stress is influenced by the stiffness of water.
- Boundary conditions: in the model, boundary conditions can be applied in terms of imposed displacements or loads.

Momentum of momentum conservation equation
- Symmetry of the stress tensor: the continuum considered here is a non-polar continuum, and hence symmetry of the stress tensor holds.

Structure of equations

The equations used in the model fall under three main categories

(*a*) General laws of conservation which must be obeyed in space and time, including the first principle of thermodynamics (e.g. equation 2).
(*b*) Constitutive relationships of the concrete describing the real behaviour of the material derived directly from experiments fulfilling also the second principle of thermodynamics.
(*c*) Thermodynamic state equations allowing the treatment of dry air and moist air as ideal gases (Clapeyron's law) as well as equilibrium relations for capillary menisci (Kelvin's Law) and gas phases (Dalton's Law).

Given the complexity of these equations, the structure of the three foregoing categories of equations is introduced in Fig. 21 to help the reader follow these equations. Each equation is divided into 'terms' and these are treated and explained individually in relevant tables to highlight their role and meaning. The general structure of terms in the constitutive relations is also illustrated in Fig. 21(b).

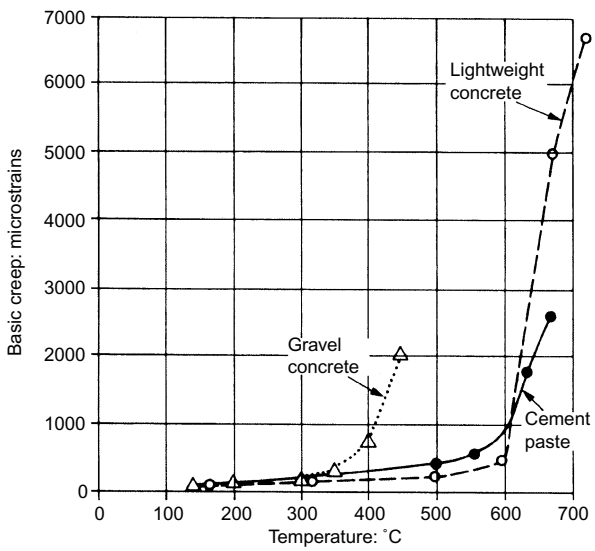

Fig. 20. Effect of temperature upon the 'basic creep' of two unsealed concretes and cement paste[32]

Conservation equations

A complete mathematical model of concrete at high temperatures will need to fully integrate (couple) the following conservation relationships (Table 7)

- Energy conservation (equation (2))
- Solid mass conservation (equation (3))
- Fluid mass conservations (equations (4 and 5))
- Linear momentum conservation (equation (6))
- Angular momentum (momentum of momentum) conservation (equation 7)

Table 7 summarises the subdivision of the conservation equations by physical constituents of concrete as modelled in this work, and presents their meaning.

Energy conservation equation. The energy conservation equation (enthalpy balance—1st law of thermodynamics) for a unit volume for all the constituents of concrete (solid and fluid) is given in equation (2) in a developed form of the basic Fourier equation[12,14]

$$fC_p\frac{\partial T}{\partial t}+[C_{pw}\rho_w\mathbf{v}_l+C_{pgwa}\rho_{gwa}\mathbf{v}_{gwa}]\nabla T-\nabla(\lambda_{eff}\nabla T)$$
$$=\Delta h_{phase}\left[\phi\frac{\partial}{\partial t}(S\rho_w)+S\rho_w\frac{\partial\phi_{hydr}}{\partial t}\right.$$
$$\left.+\alpha S\rho_w\frac{\partial}{\partial t}(\nabla u)+\nabla(\rho_w\mathbf{v}_l)\right]+\Delta h_{hydr}\frac{\partial}{\partial t}(\Delta m_{hydr}) \quad (2)$$

which, for the control volume, takes into account the following items in the order they appear in the equation—term by term—including the items inside the square brackets: (2-a) heat capacity of the concrete (solid, liquid and gas); (2-b) heat transfer by water flow (advection) into and out of the control volume; (2-c) heat transfer by moist air flow (advection) into and out of the control volume; (2-d) heat conduction (Fourier relation) into and out of the control volume; (2-e) heat released/absorbed during phase changes of evaporation/condensation; (2-f) heat released/absorbed during hydration/dehydration; (2-g) heat released/absorbed during deformation; (2-h) heat released/absorbed during sorption/desorption; (2-i) heat released/absorbed during hydration/dehydration rate change.

Solid mass conservation equation. The solid skeleton mass conservation equation for a unit volume is given as follows[12,14]

$$\frac{\partial}{\partial t}[(1-\phi)\rho_s]+\nabla[(1-\phi)\rho_s\mathbf{v}_s]=\frac{\partial}{\partial t}(\Delta m_{hydr}) \quad (3)$$

which takes into account, term by term in the order of appearance in the equation, the change of mass in the control volume due to: (3-a) change in density/porosity; (3-b) solid displacements; (3-c) hydration/dehydration.

Fluid mass conservation equations. The fluid mass conservation for a unit volume is covered by two equations, one for the dry air (equation (4)) and

(a) Independent conservation equations (2–6)					
e.g. Solid mass conservation equation (3)	Term 3-a $(\partial/\partial t)\ [(1-\phi)\rho_S]$	+	Term 3-b $\nabla[(1-\phi)\rho_S v_s]$	=	Term 3-c $(\partial/\partial t)(\Delta m_{hydr})$

(b) Constitutive relations Material dependent	Term	=	Parameter	×	Operartor	State variable
Relates term in conservation equations (2–7) with state variables via math operators			Levels 2–3		$\partial/\partial t$ (time rate) ∇ (space gradient) ∂ (differential)	Tables 2–3 Main and secondary
Example e.g. term 2-a	$\rho C_p(\partial T/\partial t)$	=	ρC_p	×	$\partial/\partial t$	T

(c) Thermodynamic state equations* Water–Dry air–Vapour–Moist air							
Type a (Clapeyron)	State variable 1	=	Parameter	×	Constant	×	State variable 2
Type b (Dalton Law)	State variable 2	=	State variable 4	+	State variable 5		

Fig. 21. Structure of the three key categories of equations in the mathematical concrete model: (a) general law conservation equations; (b) constitutive relationships; (c) thermodynamic equations
* *Kelvin's equation is an additional thermodynamic relation to generate relative humidity RH*

Table 7. Meaning of conservation of energy, mass and momentum in concrete

Item	Constituent	Sub-constituents	Conservation equation	Comments
Energy			2	Energy in solid, liquid and gas
Mass, solid		Solid matrix (skeleton)	3	Mass conservation of solids
Mass, fluid	Gas phases	Dry air Water vapour Moist air	4 5 4	Mass conservation of gas phases
	Liquid phases	Capillary water (free water) Physically adsorbed water Chemically bound water	5 5 5	Mass conservation of liquid phases
Momentum	Linear		6	Equilibrium in solid, liquid and gas
	Angular		7	Equilibrium in solid, liquid and gas

the other for water in its various forms (equation (5)).

The dry air conservation equation is as follows[12,14]

$$\phi\frac{\partial}{\partial t}[(1-S)\rho_{ga}] + (1-S)\rho_{ga}\frac{\partial\phi_{hydr}}{\partial t} + \alpha(1-S)\rho_{ga}\frac{\partial}{\partial t}(\nabla\mathbf{u}) + \nabla(\rho_{ga}\mathbf{v}_{gwa}) + \nabla(\rho_g\mathbf{v}^d_{gw-ga}) = 0 \quad (4)$$

which, for the control volume, takes into account the following items in the order they appear in the equation—term by term: (4-a) the capacity to gain/lose

dry air; (4-b) the capacity to gain/lose dry air resulting from hydration/dehydration process; (4-c) the capacity to gain/lose dry air resulting from deformation of the solid; (4-d) the amount of dry air gained/lost because of Darcian flow; (4-e) the amount of dry air gained/lost because of Fick's diffusion flow.

The water conservation equation is as follows[12,14]

$$\begin{aligned}\phi\frac{\partial}{\partial t}[(1-S)\rho_{gw}] + (1-S)\rho_{gw}\frac{\partial\phi_{hydr}}{\partial t} \\ + \alpha(1-S)\rho_{gw}\frac{\partial}{\partial t}(\nabla\mathbf{u}) + \nabla(\rho_{gw}\mathbf{v}_{gwa}) \\ + \nabla(\rho_g\mathbf{v}^d_{ga-gw}) = \\ -\phi\frac{\partial}{\partial t}(S\rho_w) - S\rho_w\frac{\partial\phi_{hydr}}{\partial t} - \alpha S\rho_w\frac{\partial}{\partial t}(\nabla\mathbf{u}) \\ - \nabla(\rho_w\mathbf{v}_l) - \nabla(\rho_w\mathbf{v}_b) - \frac{\partial}{\partial t}(\Delta m_{hydr})\end{aligned} \tag{5}$$

which, for the control volume, takes into account the following items in the order they appear in the equation—term by term: (5-a) the capacity to gain/lose water vapour in the gas phase; (5-b) the capacity to gain/lose water vapour resulting from hydration/dehydration process; (5-c) the capacity to gain/lose water vapour resulting from deformation of the solid; (5-d) the amount of water vapour gained/lost due to the Darcian flow of gas; (5-e) the amount of water vapour gained/lost because of Fick's diffusion flow; (5-f) the capacity to gain/lose water; (5-g) the capacity to gain/lose water resulting from hydration/dehydration process; (5-h) the capacity to gain/lose water resulting from deformation of the solid; (5-i) the amount of liquid gained/lost because of Darcian flow and capillary effect of free water phase with $l = w$; (5-j) the amount of liquid gained/lost because of Fick's diffusional flow for the adsorbed water phase with $l = b$; (5-k) the amount of water gained/lost because of hydration/dehydration.

Momentum 'mechanical' conservation equations—linear momentum conservation equations. The linear momentum (or mechanical equilibrium) equation is expressed as follows

$$\nabla\frac{\partial\boldsymbol{\sigma}}{\partial t} + \frac{\partial\rho}{\partial t}\mathbf{b} = 0 \tag{6}$$

which, for the control volume, takes into account the following items in the order they appear in the equation—term by term: (6-a) the external stress on the six faces of the control volume; (6-b) the internal body forces per unit volume (i.e. weight per unit volume).

Momentum 'mechanical' conservation equations—angular momentum conservation equations. The angular momentum (or momentum of momentum) equation is expressed as follows

$$\sigma_{ab} = \sigma_{ba} \tag{7}$$

which means the reciprocity of shear stresses in a non-polar continuum (i.e. symmetry of the stress tensor).

Numerical solution

Assumptions

Discretisation. The numerical picture of the thermal, hydral and mechanical phenomena is carried out by means of discretised methods which are: finite element method in space and finite difference in time.

Coupling. The most appropriate modelling approach—adopted in this article—is to fully couple all three thermal, hydral and mechanical components that are essentially fully interactive. Coupling matrices of different transport mechanisms are assembled in a single hypermatrix whose individual terms can be of several orders of magnitude different from each other. For example, mechanical stiffness can be of the order of 10^{10} but fluid permeability terms can be of the order of 10^{-18} in the same system of units leading to an ill-conditioned matrix. During heating, the occurrence of spalling can reverse the situation completely. Hence particular techniques are needed to cope with the resolution of this kind of reversing large discrepancy by adopting reconditioning techniques of the matrices involved.

Monolithic coupling approach. Since the conservation equations are fully coupled, a monolithic or a partitioned approach,[27] is required for the solution of the system of equations. A monolithic approach, used in this model, considers the whole system of equations in one stage for solution. In contrast, the partitioned approach provides the same solution in two or more stages, which could be faster with parallel computers. Large discrepancies and their reversal are accommodated in the monolithic method using conditioning coefficients.[35]

Space discretisation of conservation equations. The Galerkin method is used to convert the conservation equations from the continuum to a discrete domain, since a full variational method is not possible for the highly non-linear problem encountered in heated concrete. This method is preferred because it allows the description of geometries of any shape, and provides accurate and stable representation of the state variables and derived quantities.

Space discretisation of state variables and geometry. Shape functions describe the geometry and the state variables inside a finite region of the domain (i.e. finite element). They are usually polynomials

defining the variations of the state variables (e.g. temperature) and geometry (e.g. curved boundaries) in space. This is the main advantage of this method over the finite difference method. In this article, quadratic eight-noded finite elements are used for their versatility in accommodating complex geometries and state variables when compared with, say, stiffer four- or three-noded elements. The choice of eight nodes is adequate for modelling heated concrete, and higher power shape functions are not necessary.[36]

Finite element mesh. The finite element mesh appropriate for heated concrete is one which is fine near the heated surface and becomes coarser away from the heated surface. This is usually the case for thermal modelling because, apart from nuclear heating and few other examples, the heating is imposed upon the surface and the temperature gradient is largest near that surface. However, the peaks of moisture and pore pressure migrate inwards with progress of time. In other words these peaks vary with both space and time. Ideally, they should be modelled by a adaptive moving finite element mesh. A two-mesh approach may be the most effective and efficient method of representation and can be achieved with the partitioned approach for the solution of the system of conservation equations as explained above. Since a fixed graded finite element mesh is used in this work, the problem of the moving fronts is addressed by employing a generally finer mesh up to the necessary depth for the individual case being modelled.[37]

Numerical integration scheme. All the discretised matrices and vectors require numerical integration. In this work the standard 3×3 Gaussian integration scheme is employed for the thermal and fluid equations, but a 2×2 scheme is used for the mechanical equations, because a 3×3 scheme is too stiff in such a case.

Time discretisation. The variation with time of the state variable and derived quantities is modelled by discretising in time the system of differential conservation equations using the finite difference method. In this work a fully implicit (backward difference) linear finite difference scheme is adopted which, although conditionally stable, can converge successfully with not a very small time step length as required for less stable methods of time integration (e.g. explicit method). Unconditionally stable methods are not available for strongly non-linear problems. To ensure accuracy and stability of the solution, the time step length is limited according to standard procedures. However, in strongly non-linear problems, as encountered in heated concrete, a reduction of the minimum time step length is required depending on the degree of non-linearity at a given time step in a given point e.g. during sorption where a steep moisture gradient can exist inside one element. For this purpose the criterion adopted here is to halve the time step length repeatedly until the residual values reduce to a given tolerance.

Non-linearities. Exposure of concrete to high temperatures and pressures results in significant non-linearities of material properties (e.g. a peak in the heat capacity when $Ca(OH)_2$ dissociates at 400°C, a large increase in creep at certain temperatures, spalling etc.), thus necessitating an appropriate numerical treatment leading iterative procedures within each time step. For this purpose a full Newton–Raphson method is adopted because of its powerful ability to provide accurate results with the minimum number of iterations.

Software. A finite element programme, called HITECOSP, has been written in FORTRAN 90. It is available for several computer platforms such as PC, workstations and mainframes. It is not yet available for parallel computers but initial experiments have already commenced. Graphical interface post-processors are chosen for representing the results in PCs, workstations and mainframes. The outputs from all these are similar in terms of colour/contour maps combined with animations.

Examples of model output

Calculations using an early development version of the HITECOSP software are given in this section for a tunnel lining segment. Output from the model of gas pressure is also compared with experimental results. These are 'first cut' calculations presented here as an exercise to demonstrate what could be achieved with this software.

Comparison of model with experiment

The HITECO software output was compared with tests carried out by Pierre Kalifa of CSTB, France.[38] He developed a technique for measuring the moisture content in heated concrete using gamma-ray spectrometry which determines the change in density of concrete due to water loss. In an upgraded experiment he measured pore pressures inside the specimen. Temperature and vapour pressure fields were obtained experimentally and compared with the output from the numerical simulation. The specimens were prismatic ($30 \times 30 \times 12$ cm^3). They were provided with thermocouples for temperature measurement, and pressure gauges installed during casting.

The thermal load was applied on one face of the specimen, whereas the lateral faces of the specimen were heat-insulated with porous ceramic blocks. Heating was provided by means of a radiant heater (up to 5 kW and 600°C) that covered the surface of the

specimen, placed 3 cm above it. The temperature of the radiant heater was 600°C.

This quasi-unidirectional configuration is fairly close to that of a portion of a wall heated on one side and is properly described by the finite element mesh shown in Fig. 22. Furthermore, the imposed boundary conditions were mixed radiative–convective at the heated face. The initial internal relative humidity was 70%. In Fig. 23, the measured and calculated pressures are compared at different points inside the sample. Maximum values of pressures at different times, as well as slopes in the ascending part, agree fairly well. Also the descending branches are comparable even though the slopes do not exactly superimpose. It must be noted that the conditions in the experiment were not rigorously known (e.g. convective and radiative conditions). On the other hand, in the model, the sorption–desorption isotherms were extrapolated above the 100°C data obtained from the literature. The temperature fields also compare fairly well.

Numerical simulation of a tunnel segment exposed to fire

Calculations were performed on a curved C90 HPC concrete tunnel segment (100 mm thick) exposed to three different heating regimes. The geometry and discretisation of the tunnel segment are presented in Fig. 22. The structure was subjected to three different heating regimes for reasons of exercise: (a) ISO fire curve simulation; (b) a step temperature change to 500°C; and (c) slow heating rate at 2°C/minute. In the first and third cases mixed thermal boundary conditions (e.g. radiative and convective) have been used with a heat exchange coefficient $\alpha_c = 18\mathrm{W/m^2{}^\circ C}$ and a mass exchange coefficient $\beta_c = 0{\cdot}18$ m/s, while in the second case a constant temperature of 500°C was imposed from a radiative heat source with the same mass exchange coefficient. In all cases, the values of environmental gas pressure and relative humidity were exactly the same (e.g. $p_g = 1$ atm and RH = 50%). The initial relative humidity and temperature of concrete were 50% and 20°C respectively. Preliminary results for the ISO-fire heating regime are shown in Fig. 24. Fig. 25 shows a comparison of the results for the three heating regimes. In the first two examples, the calculation was stopped when the temperature front reached the opposite face of tunnel lining.

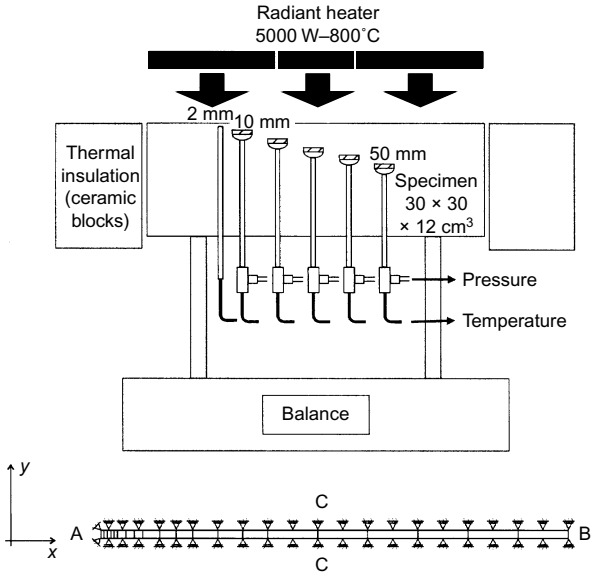

Fig. 22. Experimental set-up[39] and finite element mesh

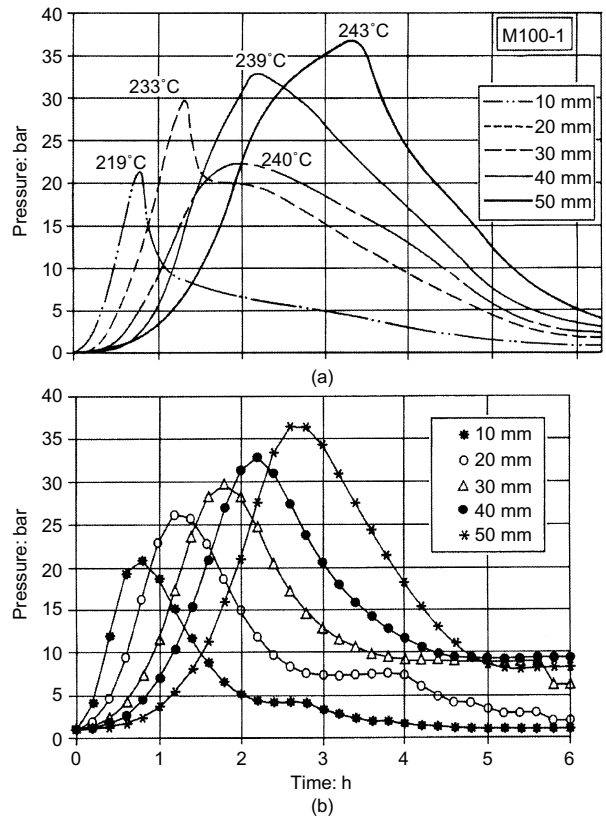

Fig. 23. Comparison of: (a) pressures measured by experiment; (b) model output pressures

Discussion

The discussion is presented below in general with particular advances made by this work, as well as the limitations, highlighted.

Experimental data

Advances. It is important to emphasise that the model described herein is a 'mechanical' model that relies for each and every mathematical term upon test results conducted on concrete, water, etc., in the laboratory. There are no terms that have been introduced 'mathematically' without foundation in reality

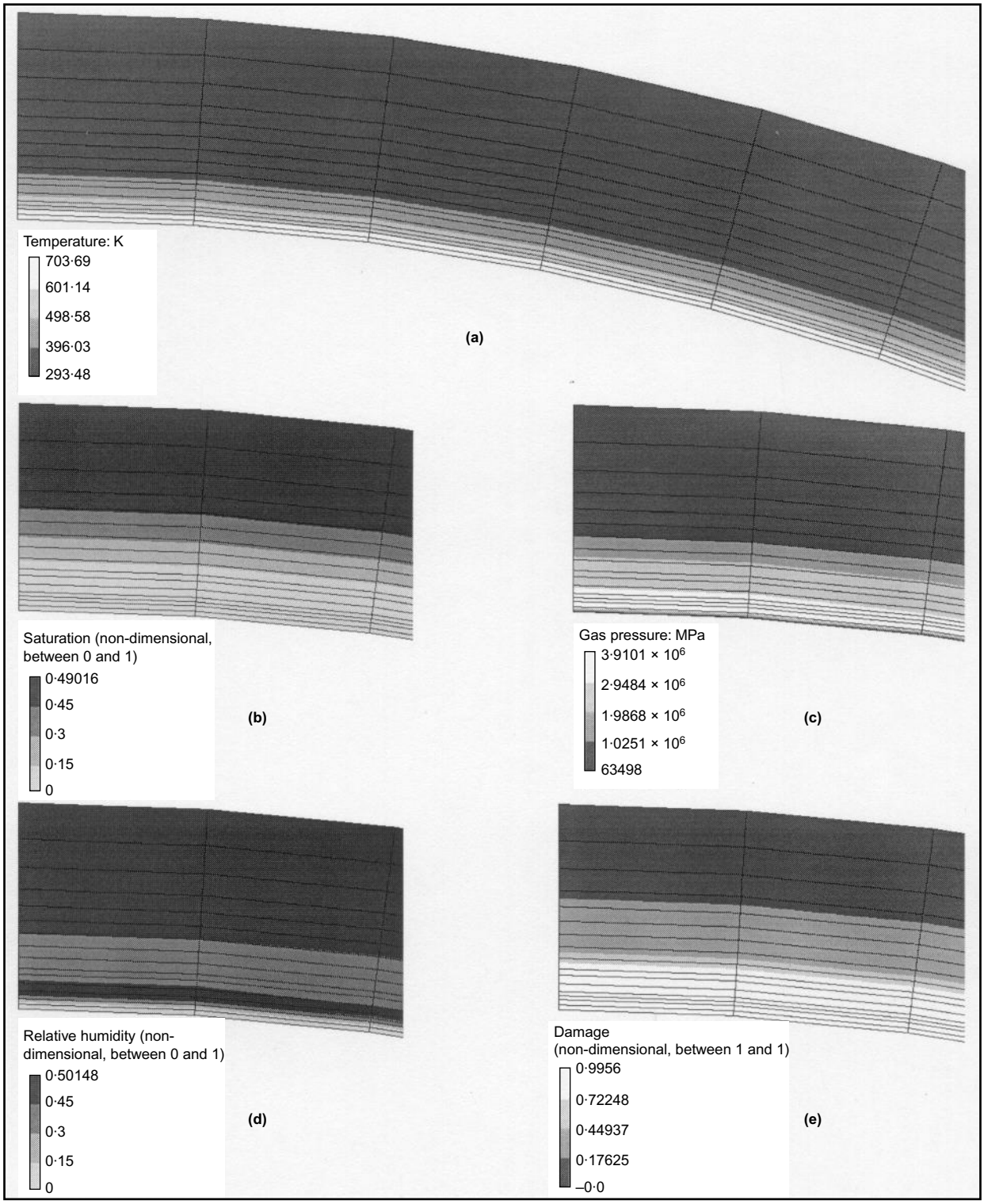

Fig. 24. Conditions within tunnel lining segment after 12 minutes exposure to ISO fire on the concave surface: (a) temperature distribution; (b) saturation distribution; (c) gas pressure; (d) relative humidity; (e) damage

from experiment. A considerable amount of thermal/mechanical/hydral/microstructural tests were carried out at different laboratories in a number of European countries on seven high performance and ultra-high performance concretes.[1] The data from these tests were input into the numerical model. In addition, data were obtained from the literature for the characteristics of water vapour and the behaviour of 'normal'

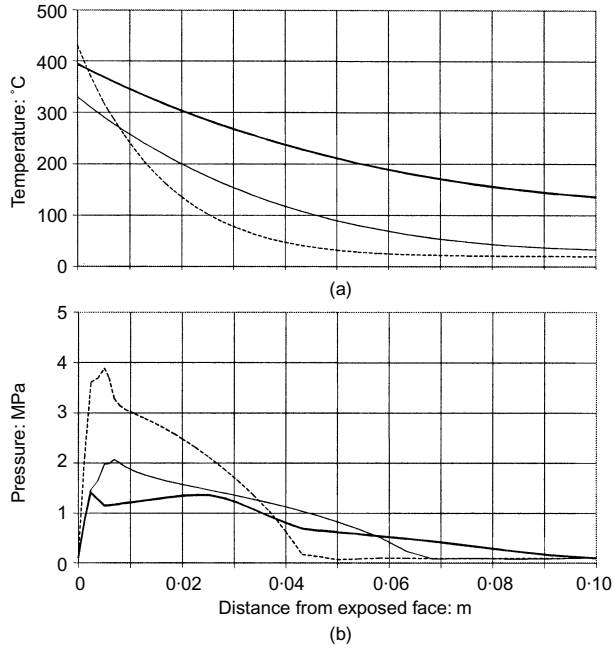

Fig. 25. (a) Temperature and; (b) vapour pressure distributions for the three heating regimes

concrete. It is important to point out that the mathematical modelling capabilities normally run ahead of the experimental data. Incorporating modelling refinements without the availability of test data may not be productive.

Limitations. While the mechanical properties (stress–strain and transient creep) were measured 'hot' during heating and 'residual' after cooling, the hydral and microstructural properties were determined only after cooling (e.g. permeability, porosity, water absorption) because test equipment available in the laboratories was designed only for testing at room temperature. Consequently, the residual permeability test results produced unrealistic pressures when predicted from the model. To overcome this problem, Khoury[40] carried out 'dynamic' permeability type tests on specimens during the heating-up stage. Another limitation is the absence of any sorption–desorption data for concrete at high temperature. This was overcome by comparing the model results with experimental results by Kalifa *et al.*[37] and by adjusting the sorption isotherms to achieve the best agreement in terms of the velocity and gradient of the water front. Nevertheless, sorption–desorption tests at high temperatures should be carried out in the future.

Multi-phase fluid

Advances. Another important point to make is that this model separates out the processes of the constituents of the fluid in terms of dry air, water vapour and the different forms of water. Previous models,[15] have considered a mixture of all the fluids as one phase.

Limitations. The 'interlayer' water phase is not included in the model nor is the non-hygroscopic water divided into two components using the concept of the irreducible saturation point.[39] Whether such refinements are necessary is still to be proven.

Heat transport processes

Advances. Heat transport by motion of fluids and solids is incorporated for the first time. Heat generated by phase changes in concrete are also incorporated for the first time. This is done for both by means of terms in the energy conservation equation.

Fluid transport processes

Advances. At a finer level, the model considers for the first time mass transport of individual fluids and the energy they carry during their motion that contributes to thermal diffusion. It also becomes possible to ascertain the relative importance of individual fluid flows at different temperature levels for different pressure gradients. In modelling vapour diffusion, another advance is that the model considers the number of collisions of water molecules in very narrow pores with the solid matrix to be non-negligible compared with the number of collisions with air molecules, thus 'Knudsen' effects are considered.

Limitations. The movement of the fluids in the pore system can be improved by incorporating the 'percolation' theory.[41]

Transport processes—Navier Stokes

Both the thermal and fluid transport processes mentioned above could be more completely described by means of the Navier Stokes equation. This allows both laminar and turbulent flows to be incorporated. However, the reason this has not been included in the model is that the Fourier heat conduction equation and the Darcy/Ficks equations are adequate for the modelling of heat and fluid transfer in concrete where the small pore structure precludes laminar and/or turbulent flows.

Separate phase changes

Advances. Previous models,[2] do not incorporate within their transport mechanism equations the individual phase changes (e.g. evaporation–condensation, hydration–dehydration, sorption–desorption) but introduce such effects as part of the global material behaviour (e.g. a peak in heat capacity at about 100°C rather than consider this change as the change in the heat capacity of the water component at different combinations of temperatures and pressures). Phase changes in concrete are, for the first time, incorporated directly in the transport mechanism of any con-

crete model. Melting and evaporation of pp fibres are modelled as phase changes.

Limitations. In a more refined model, phase changes of individual solid constituents could be included such as the dissociation of CSH, CH, aluminate, carbonate phases etc.

Consistency

Advances. In some previous works, moisture in air is described by 'relative humidity (RH)' which even sometimes appears to be > 1 because of the definition used is that of $\mathrm{RH} = p/p_s$ (p = average pressure of fluid which is not separated out, and p_s = saturation pressure). To avoid any such confusion, in this work we refer only to pressures of individual fluids and pore saturation ($0 \leqslant S \leqslant 1$). Consequently in this model the RH is never > 1.

Non-linearities

Advances. The model incorporates full non-linearities of the hydral constitutive relationships due to temperatures and pressures up to 800°C. Previous models were able to incorporate non-linearities up to about 250°C because the fluids were not separated out.

Limitations. Non-linearities caused by the presence of aggregates are not modelled but this could be overcome using this model when the finite element mesh is designed to describe the concrete at the meso-level comprising three main constituents: aggregate, cement paste and bond region. However, the characteristics of the bond region at high temperatures are not yet known.

Full-coupling

Advances. The thermal, hydral and mechanical calculations are performed in a fully interactive and coupled fashion at each iteration. For example, deformation of the solid skeleton due to thermal expansion and/or stresses will influence the fluid flows.

High performance concrete

Advances. This is the first time that a model is designed to incorporate the thermal-hydral-mechanical characteristics of HPC and UHPC. It is also the first time that the sorption–desorption curves for HPC at high temperature have been incorporated in a fully coupled concrete model.

Mechanical properties in direct tension

Advances. None of the previous models included the stress–strain data in direct tension simply because such data were not available for concrete at high temperatures. Such tests were performed at high temperature for the first time at Imperial College as part of the HITECO project and the results were incorporated in the model. This is in fact one of the main advances of the project.

Modelling damage

Advances. The direct tensile and compressive stress–strain data at high temperature for HPC are used for the first time with the isotropic Mazars damage model.[42] In other words, the model describes the complete behaviour of concrete in the elastic, inelastic and plastic ranges up to fracture. Previous models were based on elastic fracture only, see Bazant and Kaplan.[2]

Limitations. A further refinement would incorporate anisotropic or orthotropic damage models to take into account directionality of micro-fractures. Again, such data at high temperatures are not available at all.

Prediction of spalling

Advances. The model contains all the necessary basic information to allow the prediction of explosive spalling in concrete during fire.

Limitations. In its current form, the spalling criteria have not yet been included. There have been several theories describing explosive spalling presented in the past two decades but they do not as yet present a fully consistent and test proven theoretical basis.

Numerical analysis

Advances. With limited effort, the numerical model may incorporate additional physico-chemical phase changes (e.g. $\alpha-\beta$ quartz transformation) as well as the transport of other constituents (e.g. CO_2).

Limitations. The model does not currently incorporate a system to automatically check the accuracy and stability of the solution (e.g. maximum time step, or minimum number of iterations in non-linear processes to achieve convergence).

Three-dimensionality

Advances. The software is able to analyse plane stress–strain and axisymmetric problems, with reasonable computation times including problems characterised by large numbers of degrees of freedom.

Limitations. The software is not at present capable of analysing fully three-dimensional problems, but a development in that direction is under way with experiments using parallel computing being carried out.

Large strains

Limitations. The numerical formulation does not incorporate large or finite strains. Future versions will overcome this limitation.

Conclusions

It has been possible to fully couple the thermal, hydral and mechanical formulations for concrete subjected to high temperatures based on data obtained from specially conducted experiments on high performance and ultra-high performance concretes. Concrete is treated as a multiphase material consisting of a solid phase, two gas phases and three water phases. The model also incorporates the effects of chemical-physical phase changes such as hydration–dehydration, evaporation–condensation, adsorption–desorption, as well as refinements such as the effect of damage on permeability and non-linearities due to temperature and pressure.

A number of experimental and modelling advances were made by this article. The stress–strain behaviour of concrete in direct tension at high temperature was determined experimentally for the first time and input into the model. The hitherto unknown microstructural, hydral and mechanical behaviours of HPC/UHPC have also been determined experimentally and the information built into the model.

It is also the first time that such a complex model has been developed with the aim of predicting the behaviour of concrete at high temperatures in general and explosive spalling in particular. The fluid phase is considered to consist of water, dry air and vapour. The water phase consists of free capillary and physically bound water. Chemically bound water is considered part of the solid skeleton until it is released on heating. The solid is fully deformable and able to experience elastic, plastic, cracking, creep, thermal and shrinkage strain processes. Both 'basic' and importantly 'transient' creep phenomena are included.

Acknowledgements

This research was carried out as part of the Brite Euram MII BRPR-CT95-0065 'HITECO' project, 'Understanding and industrial application of High Performance Concretes in High Temperature Environment', sponsored in part by the European Commission. A partial support has been given for the second author by MURST—COFIN 1999, 'Analysis of High strength concrete'. The authors acknowledge Professor D. Gawin for his valuable contribution in the model formulation and M. Giannuzzi for software developments.

References

1. KHOURY G., ALGAR S., MAJORANA C., SCHREFLER B., KALIFA P., CHEYREZY M., BEHLOUL M., AARUP B., GIANNUZZI M. and CORSI F. Scientific summary of the HITECO research BRITE programme. *ACI International Conference on 'State-of-the-art in high performance concrete'*, Chicago, 14–18 March, 1999.
2. BAZANT Z. P. and KAPLAN M. F. *Concrete at high temperatures*, Longman, London, 1996.
3. WHITAKER S. Simultaneous heat mass and momentum transfer in porous media: a theory of drying. In *Advances in heat transfer*, 13, Academic Press, New York, 1977.
4. BEAR J. *Dynamics of fluids in porous media*, Dover, New York, 1988.
5. BEAR J. *Hydraulics of groundwater*, McGraw Hill, New York, 1979.
6. BEAR J. and BACHMAT Y. Macroscopic modelling of transport phenomena in porous media. 1: the continuum approach. *Transp. in Porous Media*, 1986, **1**, 213–240.
7. BEAR J. and BACHMAT Y. Macroscopic modelling of transport phenomena in porous media. 2: applications to mass momentum and energy transfer. *Transp. in Porous Media*, 1986, **1**, 241—269.
8. BEAR J. and BACHMAT Y. *Introduction to modelling of transport phenomena in porous media*, Kluwer, Dordrecht, 1991.
9. HASSANIZADEH M. amd GRAY W. G. General conservation equations for multiphase systems: 1. Averaging technique. *Adv. Water Res*., 1979, **2**, 131–144.
10. HASSANIZADEH M. and GRAY W. G. General conservation equations for multiphase systems: 2 Mass, momenta, energy and entropy equations. *Adv. Water Res*., 1979, **2**, 191–203.
11. HASSANIZADEH M. and GRAY W. G. General conservation equations for multiphase systems: 3 Constitutive theory for porous media. *Adv. Water Res*., 1980, **3**, 25–40.
12. SCHREFLER B. A. FE in environmental engineering: coupled thermo-hydro-mechanical processes in porous media. *Arch. Comput. Meth. Eng*., 1995, **2**, 1–54.
13. BAGGIO P., MAJORANA C. E., SCHREFLER B. A. Thermo-hygro-mechanical analysis of Concrete. *Int. J. Num. Meth. in Fluids*, 1995, **20**, 573–595.
14. GAWIN D., MAJORANA C. E. and SCHREFLER B. A. Numerical analysis of hygro-thermal behaviour and damage of concrete at high temperature. *Mechanics of Cohesive and Frictional Materials*, 1999, **4**, 37–74.
15. BAZANT Z. P. and THONGUTHAI W. Pore pressure and drying of concrete at high temperature. *J. Engng. Mech. Div., ASCE*, 1978, **104**, 1059–1079.
16. VERBECK G. and COPELAND L. E. Some physical and chemical aspects of high pressure steam curing. Paper SP32-1, Menzel Symposium on 'High Pressure Steam Curing', ACI publication SP-32, 1972, pp. 1–13.
17. KOTTAS R., SEEBERGER J. and HILSDORF H. Strength characteristics of concrete in the temperature range 20°C to 200°C', Paper H1/2, 5th SMIRT international conference, Berlin, 1979.
18. HARMARTHY T. Z. Thermal properties of concrete at elevated temperatures. *Journal of ASTM Materials*, 1970, **5**, No. 1.
19. KHOURY G. A., SULLIVAN P. J. E. and GRAINGER B. N. Transient thermal strain of concrete: literature review, conditions within specimen and individual constituent behaviour. *Magazine of Concrete Research*, 1985, **37**, No. 132, 131–144.
20. KHOURY G. A. Strain components of nuclear-reactor-type concretes during first heat cycle. *Nuclear Engineering & Design*, 1995, **156**, 313–321.
21. KHOURY G. A. Mechanical behaviour of HPC and UHPC at high temperature in compression. Final HITECO BRITE report, 1999.
22. KHOURY G. A. *Transient thermal creep of nuclear reactor pressure vessel type concretes*. PhD thesis, University of London, 3 vol., 1983.
23. KHOURY G. A. and MAJORANA C. Creep of concrete at high temperature. *Proc. International Conference 'Concreep 6'*, Boston, August, 2001, pp. 181–188.
24. KHOURY G. A., SULLIVAN P. J. E. and GRAINGER B. N. Strain of concrete during first cooling from 600°C under load. *Magazine of Concrete Research*, 1986, **38**, No. 134, 3–12.
25. LANKARD D. R., BIRKIMER D. L., FONDREIST F. F. and SNYDER

M. *Effects of moisture content on the structural properties of Portland cement exposed to temperatures up to 500°F,* ACI Special Publication SP25, Detroit, 1971.
26. KHOURY G. A., SULLIVAN P. J. E. and GRAINGER B. N. Strain of concrete during first heating to 600°C under load. *Magazine of Concrete Research*, 1985, **37**, No. 133, 195–215.
27. LEWIS R. W. and SCHREFLER B. A. *The Finite Element Method in the Static and Dynamic Deformation and Consolidation of Porous Media*, John Wiley, New York, 1998.
28. KHOURY G., ALGAR S., FELICETTI R. and GAMBAROVA P. Mechanical behaviour of HPC and UHPC concretes at high temperatures in compression and tension. *ACI International Conference on 'State-of-the-art in high performance concrete'*, Chicago, 14–18 March, 1999.
29. FELICETTI R., GAMBAROVA P., SORA M. and KHOURY G. Mechanical behaviour of HPC and UHPC in direct tension at high temperature and after cooling. *5th Rilem Symposium on Fibre-Reinforced Concrete, BEFIB' 2000*, Lyon, France, Sept.
30. ANDERBERG Y. *Fire exposed hyperstatic structures – an experimental and theoretical study*, Lund Institute of Technology, Lund, 1976.
31. KHOURY G. Unpublished test results of the strain behaviour of heated concrete, Imperial College, London, 2001.
32. KHOURY G. A., SULLIVAN P. J. E. and DIAS W. P. S. Deformation of concrete and cement paste loaded at constant temperatures from 140°C to 720°C. *Materials and Structures*, 1986, **19**, No. 110, 97–104.
33. GAWIN D. and SCHREFLER B. Thermo-hydro-mechanical analysis of partially saturated porous materials. *Engng.Comp.*, 1996, **13**, No. 7, 113—143.
34. SCHREFLER B. A. and GAWIN D. The effective stress principle: incremental or finite form? *Int. J. for Num. and Anal. Meth. in Geomechanics*, 1996, **20**, No. 11, 785–815.
35. LEWIS R. W. and SCHREFLER B. A. *The Finite Element Method in the Deformation and Consolidation of Porous Media*, John Wiley, New York, 1987.
36. ZIENKIEWICZ O. C. and TAYLOR R. L. *The Finite Element Method*, vol. 1, 4th edn., McGraw Hill, London, 1989.
37. ZIENKIEWICZ O. C. and TAYLOR R. L. *The Finite Element Method*, vol. 2, 4th edn., McGraw Hill, London, 1991.
38. KALIFA P., MENNETEAU D. and SALLEE H. Moisture and temperature distribution in a specimen heated on one face. Annual report CSTB 1997.
39. CHAUBE R. P., SHIMOMURA T. and MAEKAWA K. Multi-phase water movement in concrete as a multi-component system. In *Creep and shrinkage of concrete* (Z. P. Bazant and I. Carol (eds)), RILEM, 1993.
40. KHOURY G. Unpublished test results of dynamic weight loss, Imperial College, London, 2000.
41. DAIAN J. F. Condensation and isothermal water transfer in cement mortar. Part I – Pore size distribution, equilibrium, water condensation and imbibition. *Transport in Porous Media*, 1988, **3**, 563–589.
42. MAZARS J. Description of the behaviour of composite concretes under complex loadings through continuum damage mechanics. *Proceedings of the Tenth US National Congress of Applied Mechanics* (J. P. Lamb (ed.)), The American Society of Mechanical Engineering, 1986.

Discussion contributions on tis paper should reach the editor by 6 September 2002